Summer 8-3-2020

Characterization of a Novel Double Cooled Electrode DBD Reactor for Ozone Generation

Gustavo Duarte
duarte.gustavo@student.shu.edu

Characterization of a Novel Double Cooled Electrode DBD Reactor for Ozone Generation

by

Gustavo Duarte

Submitted in partial fulfillment of the requirements for the degree

Master of Physics

Department of Physics

Seton Hall University

August 2020

SETON HALL UNIVERSITY

COLLEGE OF ARTS AND SCIENCES

DEPARTMENT OF PHYSICS

APPROVAL FOR SUCCESSFUL DEFENSE

Gustavo Duarte has successfully defended and made the required modifications to the text of the master's thesis for the **M.S.** during this **Summer Semester 2020**.

MASTER'S COMMITTEE

(please sign and date beside your name)

Mentor:
Dr. Jose Lopez — Jose L. Lopez — 8/3/20

Committee Member:
Dr. Alfred Freilich — A. Freilich — 08/03/2020

Committee Member:
Dr. Erie H. Morales — Erie Morales — 08/03/2020

The mentor and any other committee members who wish to review revisions will sign and date this document only when revisions have been completed. Please return this form to the Office of Graduate Studies, where I will be placed in the candidate's file and submit a copy with your final thesis to be bound as page number two.

Abstract

Abstract

The Dielectric Barrier Discharge (DBD) is used to generate atmospheric or higher-pressure non-thermal plasmas and has found various commercial applications such as in industrial large-scale ozone generation. Ozone (O_3) is a powerful chemical reactant that is used to kill bacteria, to deodorize and to perform water purification. The effectiveness of the DBD reactors depends on the electrode arrangements, gap lengths, dielectric materials, operating gases and feed gas quality to name a few. However, the production of O_3 is heat sensitive. In order to prevent O_3 destruction thermal cooling of the DBD is needed. The industry approach to lower the temperature in the DBD ozone generators is by water convection. This is accomplished by having water in contact with the ground electrode. The result of lowering the temperature by convection increases O_3 yield. This research shows the results of O_3 production in a DBD with a novel double cooling electrode configuration. We found a linear relationship between ozone production and the gas flow rate as the latter increases, the ozone yield decreases. We observed when cooling the inner electrode (high voltage) and the outer electrode (ground) at the same time an increase of 7 $\%$ in the ozone yield. This research shows a linear dependency between ozone production and temperature but also manifests a more complex relation between temperature and voltage.

Acknowledgements

This master thesis would not have been possible without the guidance and help of several individuals who in one way or another contributed and extended their valuable assistance in the preparation and completion of this study.

First and foremost, my utmost gratitude to Dr. J. Lopez whose guidance, support and encouragement I will never forget. I would also like to thank the committee members Dr. Alfred Freilich and Dr. Erie H Morales.

Secondly to my family, for their endorsement when I decided to enroll at Seton Hall University and for putting up with me when I encountered anxiety and frustration.

Last but not least, to my colleagues, Emmanuel I. Akinwunmi, Conner Diminick and Matthew Feurer who participated in the research.

Contents

Abstract i

Acknowledgements ii

List of Figures v

List of Tables viii

Introduction 1

1 Plasma Theory 4

1.1 Ionization Process 6

1.2 DC Discharge 8

1.3 Air Plasma Reactions 11

2 Dielectric Barrier Discharge 16

2.1 DBD 16

2.2 Electrode Configurations and Discharge Properties 17

2.3 Micro-Discharge 20

2.4 Kinetics of Ozone 25

3 Ozone Generators 28

3.1 Temperature and Frequency 28

3.2 Ozone Production in Coaxial DBD Using an Amplitude-Modulated AC Power Supply in Air 29

3.3 Comparative Experimental Analysis of Ozone Generation between Surface and Volume DBD Generators 32

3.4 Energy Conversion and Temperature Dependence in Ozone Generator Using Pulsed Discharge in Oxygen 33

3.5 Gas Temperature Effect on Discharge-Mode Characteristics of Atmospheric-Pressure Dielectric Barrier Discharge in a Helium Oxygen Mixture . . . 36

4 Setup of the Experiment **38**

5 Results and Analysis **42**

5.1 O_3 Production of Outer Electrode, Inner Electrode and Both Electrodes at the Same Time 44

5.2 $V_{(RMS)}$ 48

5.3 Other Measurements and Analysis 50

6 Concluding Remarks **54**

References **56**

List of Figures

1 States of matter vs particle energies (eV). Adapted from "Cold Plasma Material in Fabrication: From Fundamentals to Applications" (page 3) by A. Grill, New York: IEEE (1994). 1

2 Paschen curve. Adapted from https://www.eeeguide.com. 9

3 Schematic diagram of the primary chemical reactions in an air plasma. Adapted from "Rotational and vibrational temperature measurements in capillary plasma electrode" by M. Figus, Master's Thesis, Steven Institute of Technology, QC718.5.S6 F54 (2004). 14

4 Siemens' historical ozone discharge tube. Reprinted from "Poggendorff 's Ann. Phys. Chem." by W. Siemens (1857). 16

5 Schematic of a Dielectric Barrier Discharge (covering volume discharges left and right). Adapted from "Non-Equilibrium Air Plasmas at Atmospheric Pressure" (page 70) by K.H. Becker, et al. London, United Kingdom. Published by Institute of Physics Publishing, wholly owned by The Institute of Physics, London. Print, (2005). 17

6 Schematic representation of micro-discharge activity. Adapted from "Non-Equilibrium Air Plasmas at Atmospheric Pressure" (page 71) by K.H. Becker, et al. London, United Kingdom. Published by Institute of Physics Publishing, wholly owned by The Institute of Physics, London. Print, (2005). 18

7 Lissajous Figure. Adapted from "Non-Equilibrium Air Plasmas at Atmospheric Pressure" (page 71) by K.H. Becker, et al. London, United Kingdom. Published by Institute of Physics Publishing, wholly owned by The Institute of Physics, London. Print, (2005). 19

8 a) Representation of micro-discharge activity over the electrode surface. b) Representation of micro-discharge activity over the electrode surface at low frequency and high voltage. Adapted from "Ozone synthesis from oxygen in dielectric barrier discharge" by B. Eliasson, et al. Phys. D: Appl. Phys., 20 1421-1437. Printed in the UK (1987). 22

9 Schematic diagram of the experimental setup. Reprinted from "Ozone Production in Coaxial DBD Using an Amplitude-Modulated AC Power supply in Air" (page 2) by Y. Zhang, et al. Ozone: Science & Engineering. Taylor & Francis Group (2018). 29

10 Ozone concentration and production vs. Discharge power. Reprinted from "Ozone Production in Coaxial DBD Using an Amplitude-Modulated AC Power supply in Air" (page 5) by Y. Zhang, et al. Ozone: Science & Engineering. Taylor & Francis Group (2018). 30

11 Reaction pathways for ozone production. Reprinted from "Energy Conversion and Temperature Dependence in Ozone Generator Using Pulsed Discharge in Oxygen" (page 37) by L. Wei, et al. Nanchang, China. Ozone: Science & Engineering 2017, Vol. 39, No. 1, 33-3. Taylor & Francis Group (2016). 34

12 Schematic of experimental setup. 38

13 Reactor Schematic. Adapted from C. Diminick, Seton Hall alumni, Presentation material, not dated. 39

14 a) Reactor. Gustavo, Duarte. 2020. JPG file. b) Inner electrode, ceramic coated. Gustavo, Duarte. 2020. JPG file. 40

15 Reactor inner and outer electrodes. Schematic by M. Feurer, Seton Hall alumni, Presentation material, not dated. 40

16 Ozone production, cooling both electrodes at a gas flow rate of 1 L/min. Data recorded every 10 minutes. 42

17 Ozone production, cooling both electrodes at a gas flow rate of 2 L/min. Data recorded every 5 minutes. 43

18 Ozone production, cooling both electrodes at a gas flow rate of 3 L/min. Data recorded every 12 minutes. 43
19 Ozone production, cooling both electrodes at a gas flow rate of 5 L/min. Data recorded every 12 minutes. 44
20 Ozone production, cooling the outer electrode with a gas flow rate of 1 L/min. Data recorded every 15 minutes. 45
21 Ozone production, cooling the inner electrode with a gas flow rate of 1 L/min. Data recorded every 15 minutes. 46
22 Ozone production, cooling both electrodes with a gas flow rate of 1 L/min. Data recorded every 15 minutes. 46
23 $V_{(RMS)}$ output for the outer electrode cooling. Screenshot of the oscilloscope taken every 10 minutes over a period of 3 hours. 48
24 $V_{(RMS)}$ output for the inner electrode cooling. Screenshot of the oscilloscope taken every 10 minutes over a period of 3 hours. 49
25 $V_{(RMS)}$ output for both electrodes cooling. Screenshot of the oscilloscope taken every 10 minutes over a period of 3 hours. 49
26 Deposition of material in the inner electrode. Gustavo, Duarte. 2020. JPG file. 50
27 Ozone production cooling both electrodes at different gas flow rates, at same temperature. 51
28 O_3 Production for different electrodes cooling configuration. 52
29 V_{RMS} for different electrodes cooling configuration. 53

List of Tables

1 Low-lying metastable states O_2 and O. 13

2 Ground-state, two-body reactions involving O atoms. 14

3 Ground-state three-body reactions. 14

4 Two-body reactions involving electronically excited species. 15

5 Reactions including O_3, mainly two-body reactions. 15

6 Physical and Chemical reactions. 37

7 O_3 yield side by side comparison. 47

8 Current vs. Temperature. 50

Introduction

The ancient Greeks defined plasma as a 'moldable substance.' However, modern physics and chemistry defines it as the fourth state of matter. In the beginning of the twentieth century Nobel Prize winner Dr. Irving Langmuir while working on vacuum tubes was the first one to coin the term 'plasma' to describe ionized gases [1].

Matter is classified in fourth different states: ice, water, gas and plasma. Each state could be defined by the behavior of its particles in such a way as compressible or not compressible. In other words the ability to move or flow. Using a more comprehensive definition the different states can by classified by the energetic levels of the particles in a system as shown in Figure 1. Where, solids and liquids posses energies between 0.01 and 0.75 electro-volts (eV), gases posses energies between 0.01 and $3.00\ eV$ and plasma posses energies between 0.01 and $10.05\ eV$.

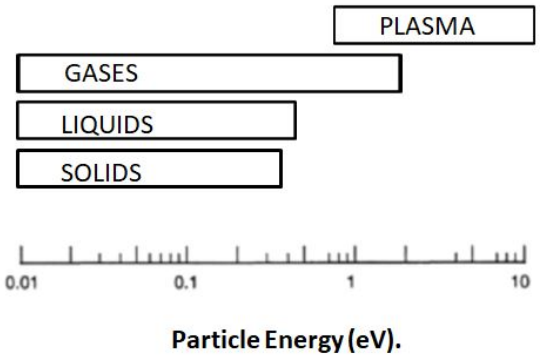

Figure 1. States of matter vs particle energies (eV). Adapted from "Cold Plasma Material in Fabrication: From Fundamentals to Applications" (page 3) by A. Grill, New York: IEEE (1994).

A more valuable definition of plasma is defined as follows: plasma is a quasi-neutral gas of charged positive and negative ions, electrons and neutral particles that possesses a collective behavior, delineated by the Kinetic Theory of Gases [2].

A specific application of cold plasma is ozone generation using a Dielectric Barrier Discharge (DBD) reactor. Ozone or trioxygen O_3 is an inorganic molecule with

symmetric bond angles of 117° and lengths of $0.128\ nm$ [3]. Because of its chemical composition O_3 is a powerful oxidizer therefore, ozone is used as a germicide. The 14^{th} International Symposium on High Pressure Low Temperature Plasma Chemistry enumerated some ozone applications such as sterilization, pest control and laser circulation system [4-6]. However, one of the most important uses of ozone is the treatment of water, waste water, reuse and industrial water application. In the Unites States, municipal waste water treatment plants (WWTPs) have been using ozone since the mid $1970s$. Currently there are 15,000 publicly owned WWTPs and about 2,700 industrial WWTPs in the United States. However, worldwide the uses of ozone as a waste treatment is limited, but there is a renewed enthusiasm in the ozone treatments and ozone potential such as disinfection of secondary effluent, sludge conditioning, odor control, pre-oxidation of primary effluent [7]. In 1987, the term "advanced oxidation" was introduced [8], the author discusses oxidation and the uses of ozone in the treatment of water sources. The outcome of ozone on Cryptosporidium was first studied in 1991 at the Colorado River water treatment facility. The most favorable disinfection of affluent of water with ozone under different conditions was reported by 1979. Furthermore, the industrial application of ozone in the last 30 years are: control of pollution, recycling marine aquaria, electroplating wastes, electronic chip manufacture, textiles and petroleum refineries. In 2001 the US FDA approved ozone as a safe agent in the treatment of malevolent microorganisms. Research is ongoing on its agricultural food applications. The research of ozone application is comprehensive in areas such as cooling tower water treatment, odor control and removal, microelectronics industry, silver recovery, medical and dental applications [9].

The Dielectric Barrier Discharge configuration is used in industrial and commercial ozone generators or reactors. However, the efficiency of the DBD reactors depends on many factors such as electrode arrangements, gap lengths, dielectric materials, operating gases and feed gas quality. However, one of the most important factors in the ozone production is the cooling of the DBD because ozone destruction reactions increase with temperature. The most common approach to cool a DBD reactor is with water flowing

in contact with the electrodes. The removal of heat from the reactor depends on input power, cooling water flow conditions, electrode geometry, reactor geometry and applied power density. The result of lowering the temperature on the reactor is the direct increase in ozone production. We create a novel reactor with a double cooling feature in order to maximize ozone capability and output.

This thesis will be organized as follows:

In Chapter 1 we will describe general introductory theory of non-thermal plasmas.

In Chapter 2 we will describe the properties of Dielectric Barrier Discharge. In order to do so we will define the basics of the theory as well as the history behind the subject.

In Chapter 3 we will conduct a literature review to find out studies concerning ozone generator configuration such as electrode arrangements, gap lengths, operating gases and electrical discharges as well as cooling system to obtain similarities and differences with the novel double cooling system.

In Chapter 4 we will discuss the experimental setup, the approach and equipment used to run the trials. A full description of the novel double cooling system will be analyzed.

In Chapter 5 we will discuss the results and present a full analysis of the output of ozone production, voltage and current will be given for the reactor configuration.

Finally, the last Chapter is a synopsis of the conclusions of the paper.

1 Plasma Theory

The kinetic theory of gases assumes that the particles of the uncharged gas are rigid spheres or radius r with density n then, we define the cross section σ, mean free path γ and the collision frequency ν as follows

$$\sigma = \pi r^2, \tag{1.0.1}$$

$$\gamma = \frac{1}{\sigma * n}, \tag{1.0.2}$$

$$\nu = \frac{\overline{v}}{\gamma}, \tag{1.0.3}$$

where $\overline{v}$ is the average velocity and defining the τ time average as

$$\tau = \frac{1}{v} = \frac{\lambda}{\overline{v}}, \tag{1.0.4}$$

follow that

$$\overline{v} = \left(\frac{kT}{M}\right)^{\frac{1}{2}}, \tag{1.0.5}$$

where T is the temperature of the system, M is the mass of the molecule and k is the Boltzman constant [10]. However, in plasma we need to account for the movement of charge particles through the medium and the concentration of positive and negative electric charges in the medium. The accumulation and movement of charge particles in plasma is responsible for the creation of Columbus forces and electromagnetic fields. The concentration of charges in a plasma are restricted to a small volume of range λ_D called Debye length. This length is defined by the following equation

$$\lambda_D = \left(\frac{\epsilon_0 k T_e}{n_e e^2}\right)^{\frac{1}{2}}, \tag{1.0.6}$$

where, ϵ_0, T_e, n_e and e are the permittivity of free space, the electron temperature, den-

sity of electrons and the electron charge. The last equation shows the following relation, λ_D decreases with the increases of the density of electrons. Furthermore, if we define a sphere of radius λ_D, we obtain a Debye sphere called N_D. Mathematically, N_D is defined as follows

$$N_D = \frac{4\pi}{3} n_e \lambda_D^3 = \frac{1.718 \times 10^9 T_e^{\frac{3}{2}} eV}{N_e^{\frac{1}{2}}}. \tag{1.0.7}$$

The last two parameters will define two conditions when an ionized gas becomes a plasma therefore

$$\lambda_D \ll L, \tag{1.0.8}$$

$$N_D \gg 1, \tag{1.0.9}$$

$$w\tau > 1, \tag{1.0.10}$$

where L is the dimension of the system [11]. However, another condition is needed in order to have a plasma which is associated with the frequency of collision in the plasma and is given by

$$w\tau > 1, \tag{1.0.11}$$

where τ is the mean time between collision of ions and neutral species.

Starting with the concept of thermodynamic equilibrium, we use the temperature of the species in the plasma to classify them. Taken in consideration several temperatures at the same time such as: T_i the temperature of the ions, T_e the temperature of the electrons, T_g the temperature of the gas related to translational energy of gas, T_{ex} the temperature of the exited particles, T_d the temperature related to dissociation, T_{ion} the temperature related to ionization, and T_r the temperature of the radiation [12]. If all the temperatures mentioned above are equal, then we achieved complete thermodynamic

equilibrium or CTE-plasmas. This kind of plasma exists only in the stars or supernova explosions. If all the temperatures mentioned above are equal, except for the thermal radiation T_r then we have plasma in local thermodynamic equilibrium or LTE-plasmas. Currently, LTE plasma with heavy energetic particles are used in fusion energy research. If the LTE-plasmas are at standard atmospheric pressure then they are described in the literature as thermal plasmas. As an example of these kinds, we have electric ark discharges and plasma jets.

If the thermodynamic equilibrium is broken then we have non-local thermal equilibrium plasmas or non-LTE. In these kinds of plasma the temperature of electrons is much higher than the ions, then we have the following relation

$$T_e \gg T_i > T_g > T_{ex}. \tag{1.0.12}$$

The electron temperature can be as high as $10\times^5$ Kelvin degrees (K) or $10\ eV$, while T_g could be as low as room temperature. Non-LTE plasma or cold plasma are at the center of much research because of its application in medicine, power generation, food industry, etc.

1.1 Ionization Process

Gas is transformed into plasma by the process of ionization. This occurs when neutral atoms or molecules become ions. The most important species in this process are positive ions and electrons. Excited electrons provide energy for the plasma. The rate of this process depends on the electron energy distribution function $f(\epsilon)$. The energy function shows the probability of an electron to have energy ϵ. Distribution function is strongly dependent on electric field and gas characteristics [13]. However, the electrons temperature play an important role on the distribution and a quasi-equilibrium is defined by the Maxwell-Boltzmann distribution function as follows

$$f(\epsilon) = 2\sqrt{\epsilon/\pi(kt_e)^3}e^{-(\epsilon/kT_e)}, \tag{1.1.1}$$

where k is the Boltzmann constant. Electron attachment to atoms or molecules gives rise to negatives ions of a charge of $-e = 1.6 \times 10^{-19}C$ the energy released during this process is defined as the electron affinity. If the atom or molecule losses an electron then we have rise to a positive ion of charge $+e$. In both cases the energy distribution function is described by the Maxwell-Boltzmann distribution function. Ionization energy (I) is the energy needed to form a positive ion. Ionization is defined as an elementary process. Therefore, ionization of species by electron impact, electron attachment or ion molecules reactions are examples of chemical reactions occurring in plasma. But also there are other reactions such as electron-ion, ion-ion recombination, excitation and dissociation of neutral species by electron impact, relaxation of excited species, electron detachment and destruction of negative ions and photo-chemical processes. The global behavior of these chemical reactions describe the plasma characteristics. In these processes, only the inelastic collision transfer energy between the species. As specified by the Kinetic Theory of Gases five parameters are needed to describes elementary process, these parameters are: the cross-section, probability, mean free path, interaction frequency reaction rate, and reaction rate coefficient. The cross section equation 1.0.1 can be idealized as an imaginary circle with area π moving in conjunction with one of the species. The probability can be defined as the ratio of the inelastic collision cross section to corresponding cross-section of elastic collision under the same condition.The mean free path equation 1.0.2 can be interpreted as the distance that one specie travels before hitting another specie. The interaction frequency of one collision partner A with partner B is given by the following equation

$$\nu_A = n_B \sigma v. \tag{1.1.2}$$

The reaction rate can be interpreted as the number of elementary processes that can occur in unit volume per unit time. It can be used for any type of monomolecular, bimolecular, and three-body reactions. The bimolecular reaction rate is given by

$$k_{(A+B)} = \int f(v)\sigma(v)vdv = \langle \sigma v \rangle. \tag{1.1.3}$$

However, the ionization rate coefficient by direct electron impact can be given by

$$k_i(T_e) = \sqrt{\frac{8T_e}{\pi m}}\sigma_0 exp\frac{-I}{T_e}. \tag{1.1.4}$$

The direct ionization rate can be expressed as a function of the reduced electric field E/n_0 which is the ratio of electric field and concentration of the species. Another important ionization process is described as the Penning Ionization in which the energy of a metastable[‡] atom A^* excited by an electron impact, exceeds the energy of an atom B therefore their collision initiates the ionization process.

1.2 DC Discharge

A DC discharge is the simplest breakdown method to obtain plasma. A DC glow discharge is produced by applying a direct current voltage between two electrodes inserted in a gas at low pressure. As the voltage is increased, the free electrons are accelerated in the electric field gaining kinetic energy. As the electrons move from the cathode to the anode they create an avalanche of electrons that ionized the gas. The avalanche is characterized by the Townsend Coefficient α rather than the ionization rate coefficient [$13^{(*)}$]. The Townsend Coefficient is defined as the electron production per unit length along the electric field. Breakdowns occur at room temperature and are inversely proportional to pressure. However, there is a secondary emission Townsend Coefficient named γ which shows the probability of a secondary release of electrons from the cathode by ion impact. This secondary Townsend parameter depends on electrode material, surfaces gas composition as well as the reduced electric field. The total current in the cathode is given by the initial electrons plus the secondary electrons emission. Furthermore, the total current in the gap is given by

$$i = \frac{i_0 exp(\alpha d)}{1 - \gamma[exp(\alpha d) - 1]}, \tag{1.2.1}$$

[‡]Metastable state: A particular excited state of an atom, nucleus, or ion that has a longer lifetime than the ordinary excited states and that generally has a shorter lifetime than the lowest, often stable, energy state, called the ground state.

where i_0 is the initial current. In order for a breakdown to occur the denominator in the last equation needs to go to zero. This occurs when the Townsend Coefficient α grows large enough. The process of ignition and self sustained current in the gap which is controlled by secondary emission is referred to as the Townsend Discharge Mechanism. The relationship between the breakdown voltage and the reduced electric field is established by the discharge gas pressure and tube dimension. However, the dependence of the breakdown voltage on gas pressure and distance can be expressed as

$$V_b = \frac{C_1(pd)}{C_2 + ln(pd)}, \tag{1.2.2}$$

where C_1 and C_2 are constants that depend on the gas characteristics, p is pressure and d is the distance in the gap [14]. The last equation expresses the relationship between voltage and (pd), which is refereed as the Paschen Law or curve as seen in Figure 2.

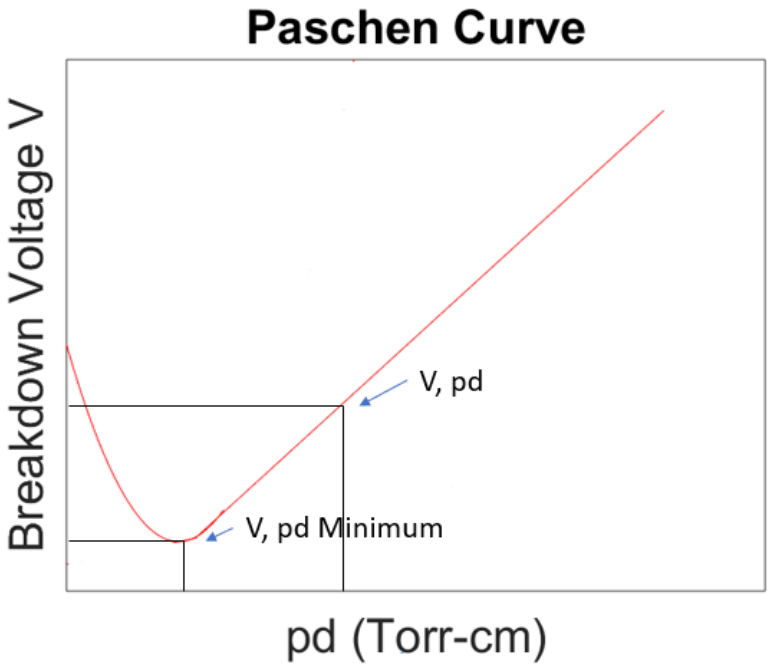

Figure 2. Paschen curve. Adapted from https://www.eeeguide.com.

The minimum point on the curve corresponds to the minimum voltage required to start the breakdown. This voltage is around $300\ V$ corresponding to an electrified of $300\ V/cm\ Torr$ and $0.7\ cm\ Torr$ for the pd. The right side of the curve shows the case when the electron avalanche has sufficient distance and gas pressure to create in-

tensive ionization even at moderate electric fields. This occurs as the pressure becomes greater than 1 $Torr$ for a gap of about 1 cm. The left side of the curve shows the case when ionization is limited by the avalanche size and gas pressure. In this case the breakdown occurs with higher electric fields. If the distance and pressure are small, the secondary electrons emitted from the cathode will not create sufficient amount of ions needed for the regeneration of secondary electrons. If the pressure is too high, then not enough energetic electrons are available to produce ions. If the distance is too large then not enough ions will reach the cathode to generate secondary emissions. Finally, we observed that the smallest the pd number the highest the voltage needed to start the breakdown.

The Townsend mechanism of breakdown occurs when $pd < 4000\ Torr$ at atmospheric pressure and $d <$ than 5 cm. If the distance in the gap is big then the avalanche is not independent and they perturb the electric field leading to a spark mechanism of breakdown. Taking into consideration the electron attachment processes, we define a new Townsend Coefficient β as follows

$$\beta = \frac{1}{\mu_e} \frac{k_a(E/n_0)}{(E/n_0)}, \tag{1.2.3}$$

where k_a is the rate of attachment coefficient. The three coefficients together describes the Townsend mechanism discharge.

The sparks mechanism occurs when the distance in the gap is large and the pressure is high. This mechanism supplies breakdown in a local narrow channel at very high currents in the order of $10^4 - 10^5\ Amp.$ and is related to electron avalanches. These narrow channels grow along the positive trail left by the primary electron avalanche. They also generate photons that initiate secondary avalanches after the initial one. In turn electrons from the secondary avalanche follow the strong electric field generated by the positively charged row of the primary avalanche. In this process, streamers that can propagate fast between anode and cathode are created. The external electric field is amplified by a strong primary electron avalanche that creates an ionized channel where the streamers grow. The avalanche change to streamer occurs when the internal elec-

tric field is comparable to the external electric field. However, if the discharge gap is small, the transformation occurs when the avalanche arrives at the anode. This streamer is called a positive streamer and grows from anode to cathode. The formation of this streamer is due to high-energy photons released from the primary avalanche providing photo-ionization that is initiating secondary avalanches. Then, electrons from the second avalanche are induced to the ionized trail of the first one and in the process create a quasi-neutral plasma. After repetitions of this process, streamers grow. Streamers grow with a velocity near of $10^8\ cm/s$. If the discharge distance is larger than the streamer, it can grow to either electrode. This kind of streamer is called negative streamer. The growth in the direction of cathode is similar to the positive streamer. However, in the anode direction the second avalanche can be initiated by electrons as well.

1.3 Air Plasma Reactions

Ionization of ground state species that are denser that other species requires a minimum energy of 10 eV. The tail of the energy distribution of electrons is capable of this ionization process due to its high energy. Taking into consideration the ionization cross section of the ground and the ionization cross section of meta-stable state, the latter requires less energy since the number of electrons with lower energy is much higher than electrons with high energy. Chemically, reactive free radicals are formed by electron impact dissociation. This process is the predecessor of chemical reactions. Random collisions between heavy particles is calculated by the coefficient rate. The probability of this rate is calculated by the velocity of the colliding species [15]. The coefficient rate depends on temperature of the heavy particles and is described by the Arrhenius Law as follows

$$k(T) = AT^n exp(E_a/k_bT), \tag{1.3.1}$$

where A is a scaling parameter E_a is the chemical reaction activation energy and n is a parameter describing the growth of the reaction versus temperature. The time span of

electron ionization and excitation is on the order of picoseconds and the electron energy distribution function reaches equilibrium in picoseconds as well. However, electron dissociative ionization and dissociation processes take nanoseconds to microseconds. At normal condition of atmospheric pressure, the duration of the chemical reactions involving ground state species is on the order of milliseconds to seconds and the free radical occurs in the order of seconds to milliseconds. The degree of ionization of air plasma is defined as follows

$$\alpha = n_e/(n_e + n_0), \tag{1.3.2}$$

where n_e is the density of electrons and n_0 is the density of neutrals species, which is on the order of 10^{-5}; this shows a weak ionization but the degree of disassociation is higher. At standard atmospheric conditions plasma chemical reactions are produced by reactions involving neutral species and ionic species.

Chemical reactions in air plasma are initiated by the ionization process on the main air plasma species O_2 and N_2

$$e^- + O_2 \rightarrow O_2^* + e^-, \tag{1.3.3}$$

$$e^- + O_2 \rightarrow O + O + e^-, \tag{1.3.4}$$

$$e^- + O_2 \rightarrow O^* + O + e^-, \tag{1.3.5}$$

$$e^- + O_2 \rightarrow O_2^+ + 2e^-, \tag{1.3.6}$$

$$e^- + O_2 \rightarrow O_2^{+*} + 2e^-, \tag{1.3.7}$$

$$e^- + O_2 \rightarrow O^+ + O + 2e^-, \tag{1.3.8}$$

$$e^- + O_2 \rightarrow O^+ + O^* + 2e^-, \tag{1.3.9}$$

$$e^- + O_2 \rightarrow O^- + O^*, \tag{1.3.10}$$

$$e^- + O_2 + M \rightarrow O_2 + M, \tag{1.3.11}$$

where * denotes an excited state and M is a third body collider. In the last set of equations, we can replace O with N and we will have the same reactions. However, in equation 1.3.11 a third body is needed to account for energy and momentum conservation [16]. For the following reactions we need to take into consideration ground-state neutrals, ions and excited species that are in a metastable state. Furthermore, accounting for the rotational and vibrational energy of the molecular species, different reaction pathways and rates of chemical reactions are observed.

Neutral species are involved in the chemical reactions at standard condition of air and pressure. In the following table, we have the low-lying and long lived metastable states of O_2 and O, which are important to the reaction of air plasma [17]. These are related to the energy needed to form them.

Table 1. Low-lying metastable states O_2 and O.

Species	State	Energy(cm^{-1})	Energy (eV)
O_2	$a^1\Delta_g$	7928.1	0.98
O_2	$b^1\Sigma_g^+$	13195	1.64
O	$1D_2$	15867.9	1.967
O	$^1S_0$	33792.6	4.190

Dry Air Plasma chemical processes are initiated by electron disassociation of N_2 and O_2, the latter requires less energy for the process. The dissociation of nitrogen and oxygen molecules into reactive radicals is a fundamental complex step in the chemical processes of air plasmas as shown in Figure 3 [18].

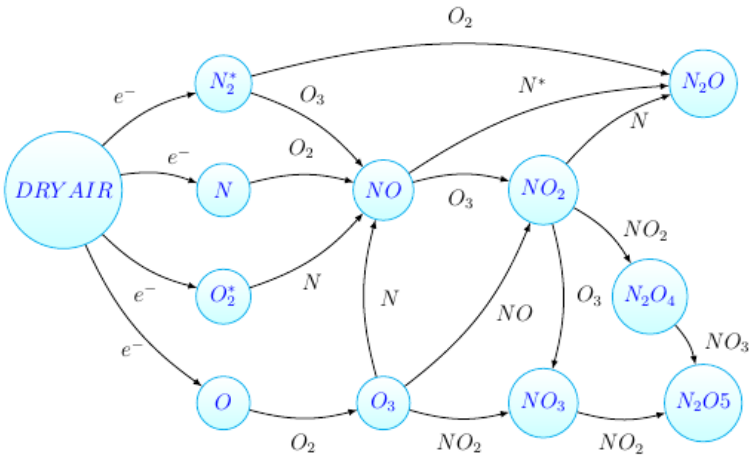

Figure 3. Schematic diagram of the primary chemical reactions in an air plasma. Adapted from "Rotational and vibrational temperature measurements in capillary plasma electrode" by M. Figus, Master's Thesis, Steven Institute of Technology, QC718.5.S6 F54 (2004).

In table 2, we present the ground state of two body reactions involving O atoms [19-20$^{(*)}$].

Table 2. Ground-state, two-body reactions involving O atoms.

Reactions	k_{298} $(cm^3\ mol^{-1}s^{-}1)$	Temperature dependence $k(T)$ $(cm^3\ mol^{-1}s^{-}1)$	Temperature Range K
$O + O_3 \rightarrow O_2 + O_2$	8×10^{-15}	$2.0 \times 10^{-11} exp(-2300/T)$	200-400
$O + NO_2 \rightarrow O_2 + NO$	9×10^{-12}	$6.5 \times 10^{-12} exp(-120/T)$	250-350

In table 3, we present the ground state of three body reactions involving O atoms.

Table 3. Ground-state three-body reactions.

Reactions	k_{300} $(cm^3\ mol^{-1}s^{-}1)$	Temperature dependence $k(T)$ $(cm^3\ mol^{-1}s^{-}1)$	Temperature Range K
$O + O + M \rightarrow O_2 + M$	9.8×10^{-14}	$4.5 \times 10^{-34} exp(630/T)[N_2]$	200-400
$O + O_2 + M \rightarrow O_3 + M$	1.6×10^{-14}	$6.0 \times 10^{-34} (T/300)^{-2.8}[O_2]$	100-300
$O + O_2 + M \rightarrow O_3 + M$	1.5×10^{-14}	$5.6 \times 10^{-34} (T/300)^{-2.8}[N_2]$	100-300

The following table (4), presents the two body reactions involving electronically excited species of O.

Table 4. Two-body reactions involving electronically excited species.

Reactions	k_{298} $(cm^3\ mol^{-1}s^-1)$
$O(^1D) + O_3 \rightarrow 2O + O_2$	1.2×10^{-10}
$O(^1D) + O_3 \rightarrow 2O_2 3(\Sigma_g^-)$	1.2×10^{-10}
$O_2(^1\Delta_g) + O_3 \rightarrow 2O_2 + O$	3.8×10^{-15}
$O_2(^1\Sigma_g^-) + O_3 \rightarrow 2O_2 + O$	2.2×10^{-11}

The table 5 below presents two body reactions including O_3 [21].

Table 5. Reactions including O_3, mainly two-body reactions.

Reactions	$k_{300}(cm^3\ mol^{-1}s^-1)$	Temperature dependence $k(T)$
$O + O_3 \rightarrow O_2(a^1\Delta) + O_2$	3×10^{-15}	$6.3 \times 10^{-12} exp(-2300/T)$
$O + O_3 \rightarrow O_2(b^1\Sigma) + O_2$	1.5×10^{-15}	$3.2 \times 10^{-12} exp(-2300/T)$

Tables 2 through 5 shows a direct temperature dependence of the rate constant. In the case of the three body reactions, the rate constant depends on temperature and gas density per cm^3, at atmospheric pressure. We also see the differences between two and three body system reactions. Furthermore, reactions with the surface material should be taken into consideration since the reaction probability, of a given chemical reaction, depends on the characteristics of the surface material and temperature. Notice that Ion-molecules kinetics affect the outcome of the chemical reactions. Ion-molecules reactions are characterized by $\langle E_{rot} \rangle$ the average reactant rotational energy, $\langle E_{vib}^{neutral} \rangle$ the average reactant vibrational energy and $\langle E_{trans} \rangle$ the average translational energy. However, these energies are more influential in chemical reactions at much higher temperatures that room temperature 300 K.

2 Dielectric Barrier Discharge

2.1 DBD

Dielectric-Barrier Discharge was introduced in 1857 by Siemens in Germany [22]. This paper proposed a novel electrical discharge that produced ozone. The Siemens configuration was arranged as follows: no metallic electrodes were in contact with the discharge plasma. Air or oxygen at atmospheric pressure was passing in the axial direction along a limited annular space in a double-walled cylindrical glass vessel. Cylindrical electrodes were located inside the inner tube and wrapped around the outer tube as seen in Figure 4. It used an alternating radial electric field with enough power to cause the electrical breakdown of the gas inside the circular discharge gap. Due to the effect of the discharge, part of the oxygen in the gas flow was converted to ozone. The glass walls have a strong effect on the discharge properties. They are referred as the Dielectric-Barrier Discharge (DBD).

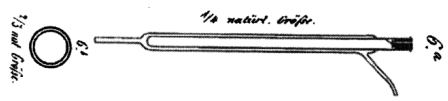

Figure 4. Siemens' historical ozone discharge tube. Reprinted from "Poggendorff 's Ann. Phys. Chem." by W. Siemens (1857).

In 1860 Andrews and Tait, suggested the name "silent discharge." At the beginning of last century important contributions were made by Warburg and Becker in industrial ozone DBD's. K. Buss acquired photographical evidence of micro-discharges and recorded current voltage using an oscilloscope. In 1943, Manley suggested a technique to find the dissipated power using a relation voltage versus charge named in today's literature as Lissajous figures [23]. He derived the power formula for ozonizers. Important contributions to understanding DBD's were made by Klemenc in 1937; Suzuki and Naito in 1952; Gobrecht et al in 1964 and Bagirov et al in 1972 [24-27]. In 1970 much research focused on understanding DBD's. Today, we use the term non-equilibrium discharge to describe this phenomenon. The main edge of DBD's is that non-equilibrium plasmas can be made in a simple and effective process at standard conditions, 1 standard

atmosphere, and 288.15 K. Because DBD's are used globally, the ozone generation market is expected to rise to 1.5 billion by 2023.

2.2 Electrode Configurations and Discharge Properties

Dielectric Barrier Discharge has different electrodes configurations, as shown in Figure 5. The main property being that one of the electrodes is insulated with a dielectric in order to limit the discharge current between the electrodes. Today, the most common configuration of the ozone reactor is the volume DBD with cylindrical structure. DBD's are AC operated and the electrode separation ranges from 0.1 millimeter (mm) to few centimeters (cm). Frequencies oscillate between 60 HZ to 300 MHz and voltages from 100 V to several kV of course variation are observed for different gases. A pressure of 10^5 Pa. is the favored range for ozone reactors. At this pressure, large micro-discharges are observed [28]. In the most high power driven DBD's one of the electrodes is cooled in order to absorb the excessive heat coming from the discharge.

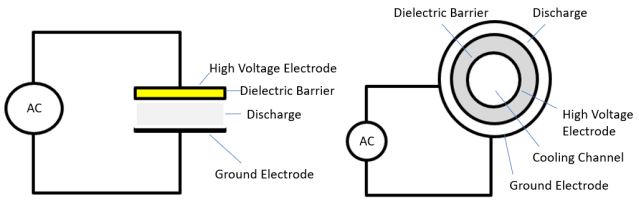

Figure 5. Schematic of a Dielectric Barrier Discharge (covering volume discharges left and right). Adapted from "Non-Equilibrium Air Plasmas at Atmospheric Pressure" (page 70) by K.H. Becker, et al. London, United Kingdom. Published by Institute of Physics Publishing, wholly owned by The Institute of Physics, London. Print, (2005).

To transfer current in the discharge gap the electric field has to be steep enough to cause a breakdown in the gas. The dielectric side of the DBD's limits the average current density in the gas space. Typically, the dielectrics are constructed with glass materials, ceramics or polymer layers. Current flow and power dissipation in DBD's occurs in short sustained micro-discharges that are recorded as average values.

When an AC voltage is applied to a DBD we have periods of discharge activity followed by discharge pauses, as seen in Figure 6. If the DBD is operated at a high

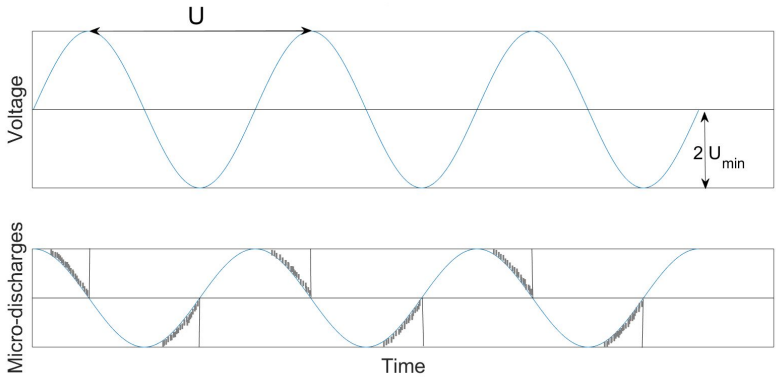

Figure 6. Schematic representation of micro-discharge activity. Adapted from "Non-Equilibrium Air Plasmas at Atmospheric Pressure" (page 71) by K.H. Becker, et al. London, United Kingdom. Published by Institute of Physics Publishing, wholly owned by The Institute of Physics, London. Print, (2005).

frequency, then the charge inside the gap won't recombine giving rise to some electrical conductivity trough the period. The voltage-charge Lissajous figure for DBD's is similar to a parallelogram as shown in Figure 7. This geometrical figure is extensively used in the ozone research literature on partial discharge [29-30]. The Lissajous parallelogram can be obtained by measuring the current and the voltage. If the peak to peak from the voltage is less than $2U_{MIN}$, then a straight line is observed and there is no discharge in the gap. Otherwise, the slope represents the total capacitance as follows

$$C_{total} = \frac{1}{\tan(\alpha)}. \tag{2.2.1}$$

When we have discharge activity in the gap, the slope belongs to the capacity of the dielectric barrier which is given by

$$C_D = \frac{1}{\tan(\gamma)}. \tag{2.2.2}$$

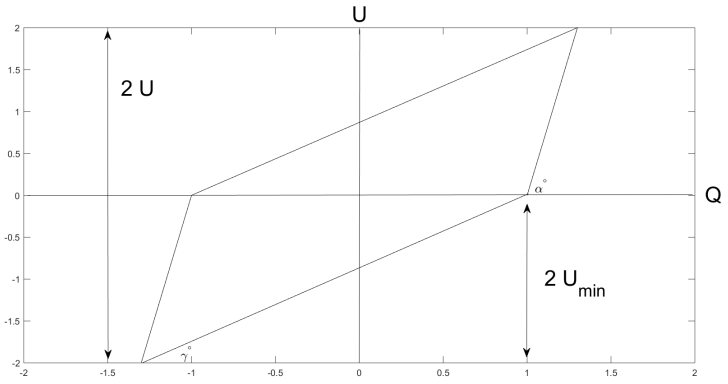

Figure 7. Lissajous Figure. Adapted from "Non-Equilibrium Air Plasmas at Atmospheric Pressure" (page 71) by K.H. Becker, et al. London, United Kingdom. Published by Institute of Physics Publishing, wholly owned by The Institute of Physics, London. Print, (2005).

The DBD electrical behavior can be represented by a simple circuit, where the discharges can be regarded as a two Zener diodes limiting the discharge voltage to $\pm\, U_{DIS}$. Where U_{DIS} represents the mean gap voltage during discharge and can be given by the following equation

$$U_{Dis} = \frac{U_{Min}}{\tan(1+\beta)}, \tag{2.2.3}$$

where $\beta = \frac{C_G}{C_D}$ and C_G is the capacitance of the gas, C_D is the capacitance of the dielectric material. Furthermore, U_D can be derived from the power equation as follows

$$P = \frac{1}{T}\int_0^T U(t)I(t)\ \mathrm{d}t = \frac{1}{\triangle T}\ U_{Dis}\int_{\triangle T} I(t)\ \mathrm{d}t. \tag{2.2.4}$$

The first integral is evaluated over 1 period T of the voltage and the second one over active discharge times. Total capacitance is given by the following equation

$$C_{total} = \frac{1}{C_G} + \frac{1}{C_D}. \tag{2.2.5}$$

The Lissajous figure demonstrates that different micro-discharges have homogeneous characteristics [23$^{(*)}$]. If the voltage in the gap is below the threshold U_{Dis} then no discharge occurs. Otherwise, micro-discharge begins in the gap before peak matching of external electric field. At this point, the displacement current along the dielectric

stops. Moreover, the area of the Lissajous parallelogram corresponds to the power sinking during the discharge cycle. The average discharge power is given by the following equation

$$P = 4fC_D U_{Dis}\,[\hat{U} - (1+\beta)U_{Dis}] = \begin{cases} for\,\hat{U} \geq (1+\beta)U_{Dis}, \\ otherwise\,P = 0, \end{cases}$$

where f is the frequency; the last equation is used for technical design of DBD's. The power formula, using U_{Dis} is as follows

$$P = 4fC_D\,(1+\beta)^{-1}U_{Min}[\hat{U} - U_{Min}] = \begin{cases} for\,\hat{U} \geq U_{Min}, \\ otherwise\,P = 0, \end{cases}$$

where $\hat{U}$ is the peak voltage. For a specified peak voltage, -power is proportional to frequency. For a specified discharge configuration and frequency the discharge starts at $U = U_{Min}$ and the power rise equivalent to the peak voltage with the following slope

$$\frac{4fC_D U_{Min}}{(1+\beta)}. \tag{2.2.6}$$

Finally, we define the average power factor $\overline{\cos(\varphi)}$ as an average quantity for a whole operating cycle of duration T. Power factor depends on the voltage form and is given by the following equation

$$PowerFactor = \overline{\cos(\varphi)} = \frac{P}{U_{eff}I_{eff}} = \frac{P}{U_{eff}I_{eff}} \int_0^T U(t)I(t)\ \mathrm{d}t. \tag{2.2.7}$$

2.3 Micro-Discharge

When the electron source production due to the process of ionization by electron impact occurs, then the detachment or photon-ionization is bigger than the drain, and an electron avalanche occurs. As the avalanche of electrons reaches a critical density the micro-discharges are created. If the electric fields $E(t)$ are changing gradually, then

the critical point is defined by the Paschen curve which is a function of the product of density n and gap distance d.

If the distance d in the gap is small in the range of $1 - 3\ mm$ stronger electric fields are needed for ignition. Time lags are observed in DBD's configurations, where the alternative electric field reaches higher values than the stationary electric field. The reduced electric field defined as E/n varies over the ranges of $100\ Td \leqslant E/n \leqslant 200\ Td$ where, $1\ Td$ or Townsend unit is equal to $10^{-17}\ V\ cm^2$ [31-32]. Time delay and the effective field are impacted by the Townsend Coefficient λ which is defined by the number of secondary electrons released from the cathode. The Townsend Coefficient varies as a function of the dielectric material and the surface properties of the electrode. The coefficient influences the micro-discharges. These micro-discharges will be initiated by Townsend avalanches if nd is small, λ is high and, slowly varying fields; otherwise the micro-discharge is started by a streamer. When micro-discharges hit the dielectric, the field is reduced because the charges accumulate at the insulator. As the field is reduced, attachment is more important than ionization and detachment; therefore, the discharge is terminated [33]. This process occurs in nanoseconds. The dielectric limits the charge of individual micro-discharges as well as makes certain that the whole electrode surface is filled with micro-discharges as seen in Figure 8-a. The oxygen breakdown and ozone production occurs only during micro-discharges. The radius of a micro-discharge is in the order of $100\ \mu$ and the properties of micro-discharge channel as follows $n = 2.4 \times 1019\ cm^{-3}$, $d = 0.1\ cm$, total charge $Q \sim 10^{-10} AS$, current density $j \sim 10^3 A\ cm^{-2}$, electron density $n_e \sim 10^{14}\ cm^{-3}$, energy density $j_l \sim 10^{-2} J\ cm^{-3}$, reduced field $E/n \sim 100 - 200\ Td$ and electron energy in the order of $5\ eV$. When a DBD has low frequency and high voltage the micro-discharges are more spreading as shown in Figure 8-b. If the DBD has low voltage and a high frequency the micro-discharges tend to repeat itself in the same channel every half period. However, the principal characteristics of micro-discharges are given by pressure, as well as the configuration and composition of the electrodes.

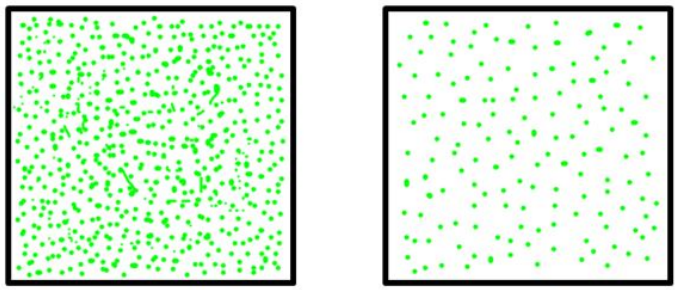

Figure 8. a) Representation of micro-discharge activity over the electrode surface. b) Representation of micro-discharge activity over the electrode surface at low frequency and high voltage. Adapted from "Ozone synthesis from oxygen in dielectric barrier discharge" by B. Eliasson, et al. Phys. D: Appl. Phys., 20 1421-1437. Printed in the UK (1987).

In order to produce ozone in a DBD reactor we need to take into consideration the evolution of different species after the micro-discharges hit the pure oxygen. Some chemical reactions limit the desirable atom concentration, degree of dissociation and maximum attainable ozone concentration. In order to achieve a better ozone yield an atom concentration of $\leq 10^{-4}$ is required. Therefore, a weak micro-discharges are needed. The micro-discharges in the reactor need to have an equilibrium between extreme energy losses (weak micro-discharge) due to ions, and eludes too many chemical reactions (strong micro-discharges). The ozone concentration rises with an increase in energy which translates into an increase of micro-discharges. Eventually, a saturation point is reached and the micro-discharges will destroy as much ozone as they yield. Saturation of ozone depends on the temperature in the gap. In order to improve ozone yield a cooling of the rector is needed.

In the dissociation process the electron excitation energy ranges from 6 to 8 eV. This is related to the electron scattering cross-section. The electron impact cross-section is used to calculate the dissociation rate coefficient. The dissociation process can be observed in the following ranges $100\,Td \leq E/n \leq 300\,Td$. Elastic collision, rotational and vibrational excitations are important for low energetic electric fields; otherwise, ionization dominates the reactions. The energy acquired by an electron per cm, in the electric field is given by the following equation

$$\Delta E = eE, \tag{2.3.1}$$

and the number of oxygen atoms produced by electron impact is given by

$$n_1 = 2\rho_7 n \nu_0^{-1}, \tag{2.3.2}$$

where ρ_7 is the dissociation rate coefficient, n the particle density of O_2 and ν_0 the drift velocity of the electrons [34]. Taking the ratio of the last two equations, we find the energy needed to obtain 1 oxygen atom. This relation shows the maximum achievable efficiency of ozone formation

$$\frac{n_1}{\Delta E} n_1 = 2\frac{\rho_7}{e\nu_d E/n}. \tag{2.3.3}$$

The saturation value of ozone formation is on the order of 0.22 O_3 molecules per eV. However, the saturation of ozone is achieved if the relative atom concentration is defined by $x_{10} = [O]/[O_2]$ is less than 10^{-4}. The relative atom concentration depends on gap separation, pressure, electrode, dielectric and gas flow level. We can define the relative atom concentration by the following equation

$$x_{10} = 2\rho_7 \frac{Q_c}{eF_c\nu_d} = 2\rho_7 \frac{Q_c}{e\nu_d (E/n)_{eff}} \frac{J_1}{n}, \tag{2.3.4}$$

where the energy density is given by

$$J_1 = \int_0^x E(t)j(t)dt = n\frac{Q_c}{F_c}(E/n)_{eff}, \tag{2.3.5}$$

where

$$Q_c = F_c \int_0^x j_(t)tdt = eF_c \int_0^x \nu_d n_e t dt. \tag{2.3.6}$$

Then, the intensity of a micro-discharge can be determined by energy density after current pulse termination or relative atom concentration.

The micro-discharge strongly depends on the temperature of the gas in the channel. An estimated upper limit of the temperature is given by the following equation

$$\Delta T_c < 0.67 J_1/\rho c_p, \tag{2.3.7}$$

therefore, an approximation of 33% is used to create ozone and a 67% will increase the temperature in the channel [35]. If we have $J_1 \approx 2\times10^{-2} Jcm^{-3}$, $\rho \approx 1.3\times10^{-3} gcm^{-3}$ and $c_p = 0.92 Jg^{-1}gK^{-1}$ then

$$\Delta T_c < 11K. \tag{2.3.8}$$

The change in temperature in the gap is proportional to the relative atom concentration and energy density but it will increase with gap distance and pressure increase. The average temperature increase in the gap is defined by the following equation

$$\Delta T_g = a(d/\lambda)(P/F)(1-\eta). \tag{2.3.9}$$

The last equation shows that the gap temperature is a balance between power and heat dissipated by cooling the reactor. Where, λ is the heat conductivity of the gas. (P/F) is the ratio between power and electrode area. Dissipating the power pseudo-equally in the volume of the discharge gap, a parabolic increase is obtained, where the coefficient a is given by $\frac{1}{3}$ for the cooling of one surface and $\frac{1}{12}$ for the cooling of both surfaces [36-37]. The factor $(1-\eta)$ accounts for the energy not used in the ozone formation. Furthermore, the average temperature can be described with the following equation

$$T_g = T_w + \Delta T_g, \tag{2.3.10}$$

where, T_w is the wall temperature. Therefore, in order to improve the micro-discharge and the ozone production an improved cooling system is needed. The cooling of the wall is achieved by water convection. In the case of the double cooling system both electrodes are cooled in order to achieve maximum heat release from the reactor.

2.4 Kinetics of Ozone

As the DBD's apply an electrical discharge onto O_2 or air, the chemical bonds between the molecule are broken and then we have subsequent reactions ending in the formation of O_3 as well as other products. The reactions have ions, electrons and CO_2 acting as reactants but the heavy charged electrons are the most active in the reactions by electron impact disassociation of O_2. The reaction scheme of ozone formation were studied by Yagi and Tanaka in 1979 [38]. In a pure oxygen discharge, ozone is produced by a three-body collision of one oxygen reacting with two O_2 molecules

$$O + O_2 + O_2 \Rightarrow O_3^* + O_2 \Rightarrow O_3 + O_2, \tag{2.4.1}$$

where O_3^* represents an initial exited state where ozone is produced; the time duration of this reactions is in the order of microseconds. When electrons react with O_2, then O is formed and after excitation the threshold energy ranges from 6 eV. to 8.4 eV. Also, there are fast side reactions where O destroys the O_3 molecules such as

$$O + O + O_2 \Rightarrow 2O_2, \tag{2.4.2}$$

$$O + O_3 + O_2 \Rightarrow 3O_2, \tag{2.4.3}$$

$$O(^1D) + O_3 \Rightarrow 2O_2, \tag{2.4.4}$$

$$O + O_3^* + O_2 \Rightarrow 3O_2. \tag{2.4.5}$$

The last four equations represent the upper limit of atom concentration and the degree of dissociation for micro-discharges. Because Equation 2.4.3 is quadratic in atom concentration then low atom concentration is expected. Models show that full concentration from O to O_3 can be achieved only if the relative atom concentration or ratio stay below 10^{-4}. If the energy density and the degree of dissociation is low in a discharge,

then $50\ \%$ of energy is dissipated in ions without any increase in ozone production. An equilibrium situation between energy losses related to ions and ozone formation is reached when the oxygen atom concentration is about 2×10^{-4} in the micro-discharge channel. This should be attained with an energy density of around $20\ mJ/cm^{-3}$ [39]. In this case $80\ \%$ of O is used in ozone formation. In order to consider the ozone formation efficiency we need to consider the enthalpy efficiency of formation given by 1.48 $eV/O_3\ m$. A $100\ \%$ ozone formation is given by formation of 0.6803 molecules per eV. The dissociation energy of $5.16\ eV$ on O_2 gives an upper limit at $0.7\ kg/kWh$. Taking in consideration the electron energy distribution in oxygen, the upper limit is given by $0.4\ kg/kWh$. The ozone concentration in the gas increases due to the accumulation action of micro-discharges. After saturation occurs, additional discharges destroy O_3 as well. Therefore, to obtain an optimal saturation concentration, an equilibrium between temperature and pressure must be obtained.

Dry air ozone formation is more complex since we have nitrogen atoms as well as excited species such as N^+, N_2^+, N_4^+, $N_2(A^3\Sigma_u)$ and $N_2(B^3\Pi_g)$. Excitation and dissociation of nitrogen molecules, can generate additional oxygen atoms for ozone generation. Then we have the following equations

$$N + O_2 \Rightarrow NO + O, \tag{2.4.6}$$

$$N + NO + N_2 \Rightarrow N_2 + O, \tag{2.4.7}$$

$$N + NO_2 \Rightarrow N_2 + 2O, \tag{2.4.8}$$

$$N_2(A, B) + O_2 \Rightarrow N_2O + 2O, \tag{2.4.9}$$

$$N_2(A) + O_2 \Rightarrow N_2O + O. \tag{2.4.10}$$

The oxygen atoms of these reactions, as well as the ones generated by direct electron impact, contribute $50\ \%$ of the ozone formation. The reactions take about $100\ \mu s$. A fraction of the energy loss, in electron nitrogen collision can be eventually recovered in ozone production, as shown in equations 2.4.6 trough 2.4.10. Besides, ozone formation produces species of nitrogen such as NO, N_2O, NO_2, NO_3 and N_2O_5 [40]. The peak of achievable energy efficiency is around $0.2kg/kW\ h$ and electric field values in the order of $200-300\ Td$. The achievable ozone concentration is lower than in pure oxygen discharges and no saturation concentration point is attainable. The discharge poisoning effect prevents the formation of O_3 and destroys molecules of ozone already in the system [41]. Furthermore, if a concentration of $0.1\ \%\ NO_x$ is added to the feed of the reactor, it may destroy or suppress ozone formation.

A more complex situation is in the case of ozone production in conditions of humidity, oxygen and air. This is because humidity changes the conductivity of the dielectric. With the same AC conditions fewer micro-discharges occur and bigger reaction paths results from the presence of OH and HO_2. The last two reactants are known to be limiting the production of ozone, due to further catalytic ozone destruction.

3 Ozone Generators

3.1 Temperature and Frequency

Experimental measurements of the gas temperature in DBD's and its evolution at different frequencies has been reported in [42]. For a frequency of $100\ Hz$ and voltage of $13.4\ kV$. The temperature of electrons increases until it reaches a steady state of $40°C$, the temperature of the gas follows the same path and reaches $30°C$. Now, for a frequency of $200\ Hz$, the steady state of electrons is reached at $58°C$ and for the gas this value is $40°C$. However, with a frequency of $300\ Hz$ the same phenomenon as before is not reported until the temperature reaches $60°C$. At this point a steep increase is reported until a steady state is reached at a value of $170°C$. The inner temperature of a gas reactor was measured and found the following; the gas temperature increases with the 'plasma on' until it reaches a steady state. However, some variations to the pattern has been detected at $65°C$ with an increase of power as well as temperature. This variation could be due to the impedance of reactor.

The temperature of the reactor increases with time and voltage. This effect produces a decrease in the ozone production. For some DBD's configurations, the ozone concentration decreases from 14 g/h to 3 g/h after 10 minutes of operation [43]. The temperature increases at different points of the reactor but is lower at the oxygen inlet than the ozone outlet. After 10 minutes of reactor operation the temperature increased from $26°C$ to $97°C$ producing an ozone decrease due to molecular dissociation. Therefore, an increase of ozone production efficiency can be achieved by cooling the system.

The cooling of ozone reactors is achieved by water convection near the electrodes. The larger systems are cylindrical in shape, with external water cooling of the electrodes; internal cooling is also used in different systems in the US. Several patents of ozone reactors were presented to the USPTO such as U.S. Patent 4614573, 3921002, 4079260 [44]. Today, ozone reactors are made of stainless steel and the cooling system may be an open or closed loop. But the latter is better for water quality. Reducing the water temperature from $35°C$ to $5°C$ could save about $30\ \%$ of energy required for

an ozone production rate. However, there is a cost associated with cooling water in the form of electrical energy operation for chillers which is most notable in the case of industrial ozone production.

3.2 Ozone Production in Coaxial DBD Using an Amplitude-Modulated AC Power Supply in Air

Zhang, et al. [45] investigated the ozone generation characteristics under different conditions such as distinct energy densities, duty cycles and air flow rates, as well as cooling conditions and frequencies. The goal of the researchers was to increase the ozone production without increasing energy consumption of the reactor. In this case, the experiment was set up as shown in Figure 9: the tubular reactor, gas-feeding unit, water cooling unit, ozone monitors, temperature sensors, discharge power supply unit and electrical diagnostics. Synthetic air was used to produce the ozone, the air flow was set as 5 slm, gas temperature at the inlet was $24.6 \pm 0.2\ K$. The pressure in the discharge gap was $760 \pm 5\ Torr$ and the temperature of cooling water at the inlet of the reactor was kept constant at $19.2\ K \pm 0.3\ K$.

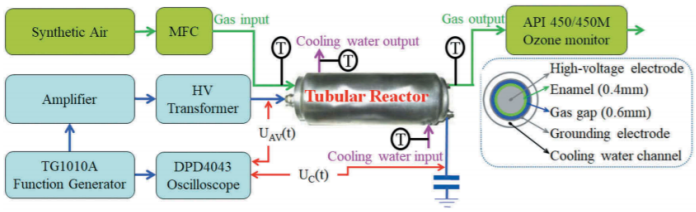

Figure 9. Schematic diagram of the experimental setup. Reprinted from "Ozone Production in Coaxial DBD Using an Amplitude-Modulated AC Power supply in Air" (page 2) by Y. Zhang, et al. Ozone: Science & Engineering. Taylor & Francis Group (2018).

The researchers discussed the results of energy density changes and its effects on the reactor ozone production. They analyzed typical voltage waveforms as well as the discharge power for each AC cycle which is represented with the corresponding Lissajous figure. The average discharge power increases with the increase of peak to peak voltage as expected. The average discharge power is lowered with water cooling in the reactor. The ozone concentration and output when the reactor is cooler with water

has a linear increase in energy density; as energy density increases to $350.71\ \frac{kj}{m^3}$ the ozone concentration and output reaches 2120 ppm and $1.74\ \frac{g}{h}$. If the ozone reactor is not cooled with water, then the relation between output ozone generation and density energy diverge from linearity as the gas temperature increases. As expected, without water cooling, the gas temperature increases. This is due to an increase in heat from the grounded electrode that can not be eliminated. Using synthetic air and oxygen in the discharge, the researchers found out that the temperature difference is higher in oxygen because more energy is needed to produce ozone. In the case of pure oxygen with an energy increase of $348.73\ kJ/m^3$ the temperature rises to $4.7\ K$. When the reactor is water cooled, there is a small increase in the air gas temperature around $1,34\ K$ and an insignificant increase in water temperature. The gas temperature in the outlet increases slowly in a long period of time. The AC frequency of $1\ kHz$ shows the following: the average ozone yield is $52 \pm 3\ g/kWh$ with ozone concentrations ranging from 518 ppm to 2120 ppm in the cooled case and $42 \pm 5\ g/kWh$ in the non-cooled case. Ozone production is higher under the water cooling conditions as seen in Figure 10. This happened because higher ozone concentration at lower temperatures.

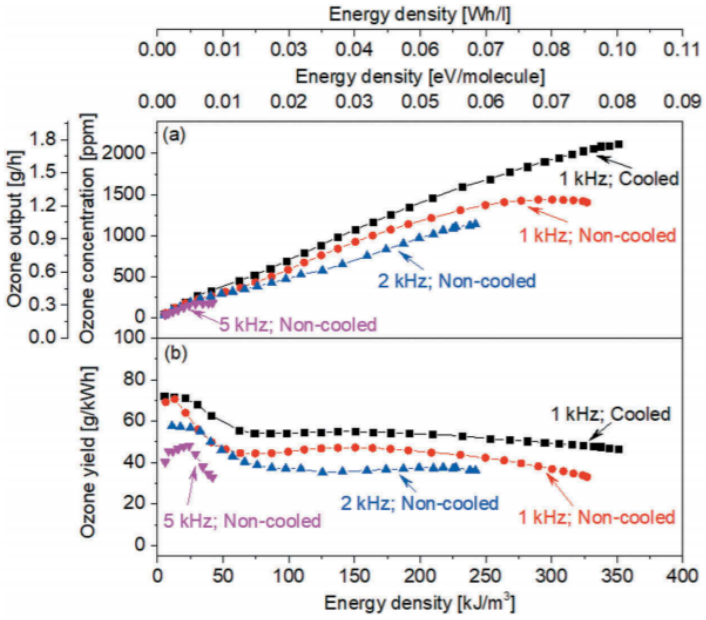

Figure 10. Ozone concentration and production vs. Discharge power. Reprinted from "Ozone Production in Coaxial DBD Using an Amplitude-Modulated AC Power supply in Air" (page 5) by Y. Zhang, et al. Ozone: Science & Engineering. Taylor & Francis Group (2018).

The general influence of duty cycle on ozone generation is as follows: when a single AC cycle in one complete period, the average discharge and ozone concentration show an initial linear increase with departure from linearity as temperature increases with higher cycles. However, ozone production is maintained almost constant in both synthetic air and pure oxygen in a different spectrum of duty cycles. In the event of several AC cycles in one period, we observed the following: for higher duty cycles, a much larger deviation and a tendency of the ozone to achieve steady state concentration and production. However, ozone production decreases in time with the increase of duty cycle. Water cooling the reactor has no effect on the positive, negative or peak to peak voltage. Furthermore, there are no significant effects with the water cooling reactor or without the water cooling at different AC frequencies. The influence of gas flow on ozone production is as follows: ozone concentration decreases as air flow increases. This is due to a shorter contact with discharge. The thermal decay of ozone production due to temperature can be neglected because of high rates of water flow through the reactor. However, ozone yield and ozone output increase gradually with increasing air flow rate. The ozone concentration and ozone yield are inversely proportional at a high discharge power and voltage. High energy electrons depend on discharge power and more ozone is produced when exited electrons avalanche through the gas. But the output is an increase in temperature and that decreases the ozone yield.

The capacitance of the reactor can be obtained by the Lissajous figure and can be separated in total capacitance, gap capacitance and dielectric capacitance. The dielectric capacitance goes up and then stabilizes as energy density increases. The gap capacitance decreases and then becomes unperturbed or constant. The total capacitance of the reactor was nearly constant at $1.78 \pm 0.02\ nF$. If the reactor is cooled, then dielectric capacitance is moderately lower and the gap capacitance is a bit higher. The total capacitance is mostly independent of water cooling conditions, energy density and frequencies. However, gas capacitance and dielectric capacitance are barely influenced by water cooling.

Ozone concentration and ozone production exhibit a linear increase with energy

density as the reactor is cooled. The linearity is broken after a certain temperature is reached. Therefore, ozone production is higher in the cooling case. Ozone concentration decreases with the increase of air flow because less contact time is allowed at the discharge. A lower dielectric capacitance and higher gas capacitance is obtained in the cooling case. The total capacitance is not affected by the cooling water.

3.3 Comparative Experimental Analysis of Ozone Generation between Surface and Volume DBD Generators

Nassour, et al. [46] researched and compared surface DBD versus volume DBD, both with cylindrical geometry and taking into account parameters such as ozone concentration, energy efficiency and cooling performance. The experiment set up was as follows: the tubular reactor (ozone generator), variable AC power supply, HV/HF transformer, piroscope, air supply and ozone monitor 106 H.

The reactors were placed inside a container for cooling purposes. Three different cooling systems were applied to the volume DBD and surface DBD. The cooling systems are described as follows: system $1-$ air ventilation using a fan, system $2-$ the container was filled with water, system $3-$ the container was filled with moving cooled water. In addition, the flow rate of oxygen was set at $(1 - 10\ L/min)$ and the experiments were done under standard conditions of temperature and humidity. The current in the VDBD is shown to be greater than in the SDBD. However, uniform micro-discharges density is obtained in the surface configuration. If the same applied voltage of 5.5 kV is delivered to both configurations the power consumed by the SDBD is smaller than the VDBD configuration. The energy consumed during one cycle was 0.855 mJ corresponding to a consumed power of 38.5 W for SDBD and 1.112 mJ corresponding to a power use of of 50 W for the VBDB.

The ozone concentration as a function of voltage, increases with applied voltage in either configuration. When voltage is greater than $5\ kV$, we observe an increase in temperature due to extra energy being transformed into heat resulting in ozone dissociation. Ozone concentration is higher in a SDBD than in VDBD because of the higher density

of micro-discharges for the surface plasma and the geometry of the mesh electrode.

When the oxygen flow rate is increased, the ozone production is increased as well. However the SDBD output is higher than VDBD. The energy efficiency representing the variation of the ratio ozone-rate/power as a function of the applied voltage shows a superior ratio in the case of SDBD.

The three systems were compared with the no cooling system in order to see the effects of temperature in ozone production. The effects of the discharge are an increase in heat, and part of this heat is removed with the cooling system. System 3 with cooling moving water was the best for both reactors VDVD and SDBD maintaining a quasi constant temperature for a period of up to 3 hours. With no cooling system the temperature rises up to $90°C$ in an hour which causes a failure of the glass tube.

The ozone concentration is higher with system 3 and it's production remains constant during the experiment. Finally, the SDBD has a better output of ozone concentration and uses less energy than VDVD. The cooling system 3 is more efficient for decreasing temperature. Therefore, is better suited for ozone production and concentration.

3.4 Energy Conversion and Temperature Dependence in Ozone Generator Using Pulsed Discharge in Oxygen

Wei, et al. [47] did a kinetic model on 11 species and 63 reactions in order to investigate energy and temperature dependency of ozone generators using pulsed discharge. They analyzed the rate of production for the most important species O_3, O, $O(1D)$ as seen in Figure 14. They estimated the temperature dependency of sensitivity coefficient and production rate for each species. The production rate of ozone is linear with the increase of temperature but also increases the destruction of ozone, therefore the gain is neutralized. It has been estimated that 20 percent of the energy is used in the production of ozone. The rest of the energy is converted into heat which dissipates through the walls of the reactor as well as increases the temperature in the gap.

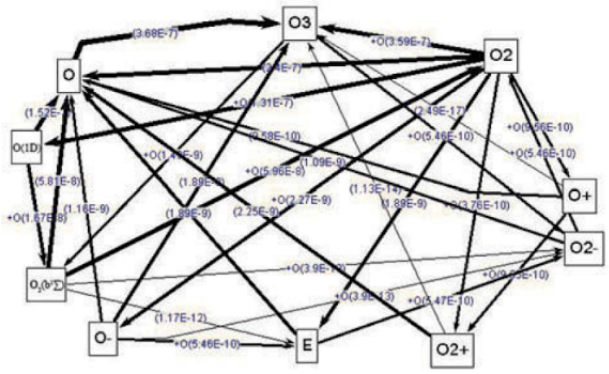

Figure 11. Reaction pathways for ozone production. Reprinted from "Energy Conversion and Temperature Dependence in Ozone Generator Using Pulsed Discharge in Oxygen" (page 37) by L. Wei, et al. Nanchang, China. Ozone: Science & Engineering 2017, Vol. 39, No. 1, 33-3. Taylor & Francis Group (2016).

Usually the energy in the reactor is divided into three parts: reaction heat, heat carried by gas and heat loss to ambient. The temperature of the gas is defined by the difference in temperature between inlet and outlet. Also, the energy conversion ratios are given by η reaction, η gas and η loss. When the inlet gas temperature changes from 298 K to 343 K then, η reaction, η gas and η loss change from 32.6 $\%$, 5.7 $\%$ and 61.7 $\%$ to 13.7 $\%$, 7.5 $\%$ and 78,8 $\%$. The decrease in the reaction is due to the increase in the temperature in the inlet gas. The gas temperature is the fundamental parameter that defines the energy efficiency. The production and destruction of ozone dependent on temperature. Therefore, the combined yield is a function of temperature. Where the reaction rates of ozone production decrease with the increase of temperature as well as the rate of ozone destruction. The rate of production is useful to determinate the contribution of each individual reaction to the contribution or destruction of species. The analysis of O_3 species at different temperatures shows that reaction R35 is the most important in the ozone production with the increase, in temperature. But reaction R2, with the same increase, creates more oxygen destroying ozone formation. The gas temperature is responsible for the reaction rate and sensibility coefficients. As the temperature increases the gas density will change and the electron temperature will change, since it is a function of the electric-field E/n. The temperature on the electron influences the reaction rates and sensitivity coefficients of reaction by ionization. Reactions R41 and

R44 increase the ozone destruction with the increase of temperature. Reactions R35 and R45 contribute the most to ozone formation. Finally, the production and destruction rate increases linearly in all reactions with the increase of temperature, showing a clear picture of the ozone temperature-production relation.

The oxygen rate of production at different gas temperatures is dominated by reactions R2 and R7. While, the coefficient reaction of R2 decreases with the increase in temperature, the coefficient reaction R7 increases with the increase of the gas temperature. Both reactions shown linear behavior with the increase of gas temperature. This is due to more energetic electrons being produced at high gas temperatures causing a peak of oxygen concentration. Reaction R35 is the main producer of ozone and oxygen destruction as temperature increases. This reaction increases the consumption of oxygen.

The $O(1D)$ rate of production at different gas temperatures is dominated by reaction R7 and reaction R44 have a high sensitivity coefficient as temperature increases. Reactions R28, R27 and R2 are responsible for significant rates of destruction and production rates of $O(1D)$. All reactions increase destruction and creation rates as the gas temperature goes higher.

The numerical results of this paper agree with the experimental data of ozone production and destruction rate for different species: η_{loss} and η_{gas} increases with the gas temperature. However, $\eta_{reactions}$ decreases with the increase of temperatures in the discharge gap. Reactions $O_3+O_3 => O_2+O_2+O_2$ and $O_3+O => O_2(b^1\Sigma)+O_2$ are the most important reactions for ozone destruction, and reaction $O+O_2+O_2 => O_3+O_2$ is the most important reaction to form ozone.

3.5 Gas Temperature Effect on Discharge-Mode Characteristics of Atmospheric-Pressure Dielectric Barrier Discharge in a Helium Oxygen Mixture

Kang, et al. [48] did a numerical study for a Dielectric Barrier Discharge in order to obtain a better understating of gas and the temperature effects on plasma characteristics. In the numerical simulation, they included temperature effects, gas heating by enthalpy change and Joule heating with ionic current movement are considered in the helium-oxygen mixture. They used 13 species and 46 reactions and changed the ambient temperature from 300 K to 500 K. There, the plasma characteristics, are calculated by the variations of the electric field, species densities in the DBD region and voltage-current characteristic curves. The simulation is carried on in a 1 dimension time dependent numerical study where the plasma is assumed to be uniformly distributed. The gap on the reactor is 3 mm, the dielectrics material is 1 mm thick and the relative permittivity is 8. The continuity equation is used to calculate the motion of ions and electrons. The Poisson equation is used to calculate electric potential and electric field. For the boundary conditions, at the barrier-plasma interface, all incoming electrons and ions are assumed to accumulate at surface charges, depending on the electric field and secondaries emission from the barrier surface and ion-electron recombination at this point. The boundary conditions for electric field and potential are calculated with the Gauss theorem with surface charges. The gas temperature is calculated by using the energy equation including enthalpy changes and Joule heating during the reactor discharge. The average gas velocity v is assumed to be constant at 5 m/s. Simulations are carried out at three different temperatures 300 K, 400 K and 500 K with a power frequency of 10 kHz and oxygen concentration of 5 ppm. At 300 K the discharge voltage gradually increases up to the breakdown voltage of the gas, the maximum current achieved is 4.2 mA/cm^2 and then there is a rapid voltage drops. At the moment of the current peak, the average density of electrons and helium metastable species is also at peak value. When the temperatures are at 400 K and 500 K, the discharge current peaks are less

than 1.4 mA/cm^2. Electron and helium densities show smaller peak values against the 300 K case. A stronger electric field and species density is observed at 300 K. The ozone density is a little higher at 500 K than 400 K and 300 K. The voltage current characteristic curve is higher for the 300 K temperature, followed by the 400 K and 500 K. At 300 K, the DBD plasma showed the typical characteristics of a self-sustaining glow discharge with increasing currents up to 4.2 mA/cm^2. When the frequency was changed from 10 kHZ, 20 khz and 30 kHZ, but the temperature was kept constant at 300 K, the density of ozone was higher in the following order: 30 kHZ, 20 kHZ and 10 kHZ. The results show that the discharge characteristics of a DBD is strongly related to temperature. Gas temperature is the principal cause of increase or decrease of species in the reactor, in particular to this case the study reactions 19 through 23, are ozone related as seen in Table 6 [49].

Table 6. Physical and Chemical reactions.

Reactions		Rate Coefficient $k(i)$
19	$O + O_2 + O \rightarrow O_3 + O$	2.15×10^{-34} exp $(345/T_g)cm^6s^{-1}$
20	$O + O_2 + O_2 \rightarrow O_3 + O_2$	$6.9 \times 10^{-34}(300/T_g)^{1.25}cm^6s^{-1}$
21	$O + O_2 + O_3 \rightarrow O_3 + O_3$	4.6×10^{-35} exp$(1050/T_g)cm^6s^{-1}$
22	$O_3 + O_2 \rightarrow O + O_2 + O_2$	7.3×10^{-10} exp$(-11400/T_g)cm^3s^{-1}$
23	$O_3 + O_3 \rightarrow O + O_2 + O_3$	1.65×10^{-9} exp $(-11400/T_g)cm^3s^{-1}$

The transition from glow to Townsend due to the temperature change can be explained by the following two-step reactions. First, temperature-dependent reaction rate coefficients increase at a high ambient temperature, and the dissociation of ozone is accordingly accelerated by the relevant reactions of the density of ozone decrease, while the densities of O and O_2 increase in the discharge region of the reactor. These increased O and O_2 species extinguish the generation of He^* species that are necessary to sustain a glow discharge state. Secondly, the density of He^* decreases, and the discharge characteristics will be changed to a Townsend mode.

The V-I characteristic curve shows the lower discharge voltage not cooling 400 K with a Townsend mode. Then, a higher discharge at 350 K and the highest at 300 K where the discharge changes to a glow mode.

4 Setup of the Experiment

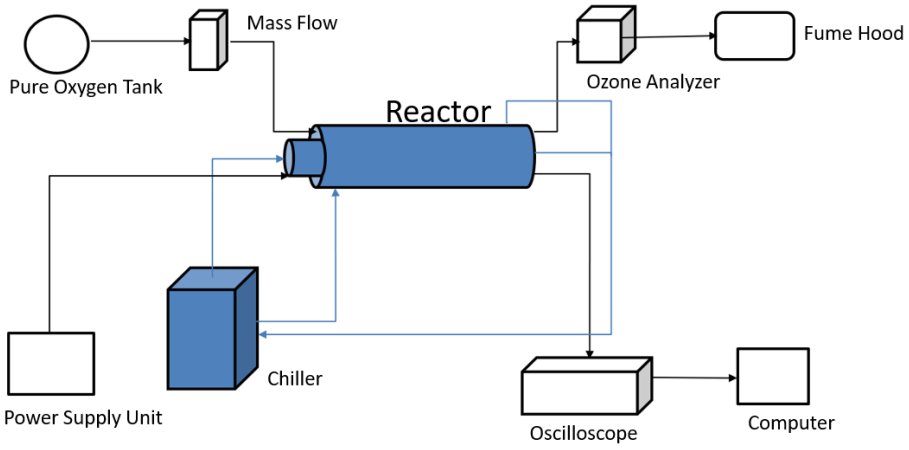

Figure 12. Schematic of experimental setup.

The experimental setup in Figure 12 is as follows: the novel cylindrical reactor has two separate cooling systems; one in the inner electrode and the other one in the outer electrode. The discharge gap was fed with pure oxygen UN 1072 research grade 99.999 %; containing 0.5 ppm of H_2O, 0.2 ppm of THC, 0.5 ppm of CO, 0.5 ppm of CO_2, 3 ppm of AR, 5 ppm of N_2 and 2 ppm of Kr. The circulation of the oxygen was controlled by a ColeParmer® mass flow controller. The ozone production was measured with ozone analyzer BMT 964-C, produced by BMT Messtechnich, Berlin. The ozone analyzer BMT 964 is fully automatic. The UV photometer measures the density $[g/m^3]$ of ozone. However, we present the data as the ratio mass ozone, mass ozone gas which is given by the following equation

$$[wt/wt] = \frac{100[g/Nm^3]}{[g/Nm^3] - \frac{\rho_r}{\rho_0}[g/Nm^3] + \rho_{ra}}, \tag{4.0.1}$$

where $\rho_0 = 2143.93\ g/Nm^3$ is the density of ozone, $\rho_r = 1498.26\ g/Nm^3$ is the density of oxygen and $\rho_{ra} = 1293.0\ g/Nm^3$ is the density of dry atmospheric air. The temperature of the water is controlled by thermo scientific NESLAB Merlin M33 recirculating chiller which is designed to provide a constant supply of cooled liquid at constant temperature and volume. A high-voltage AC power supply (PSU) is connected to the reactor terminals and used to create the discharges. The measurement of voltage

and current is done using an oscilloscope from Tektronix model MSO-4054 with the following specifications; 1 GHz, 500 MHz and 350 MHz bandwidths. The oscilloscope possesses four channels, with sample rates up to 5 GS/s on all analog channels and 10 M points record length on all channels and 50,000 waveforms per second display rate. The following probe was used in the experiment, the Tektronix P6015A 1000X, 3-meter Single-Ended High-voltage Probe. This is the industry standard for heavy-duty high-performance measurements of voltages over 2.5 kV. We used the programs Tekvisa and Open-wave to collect the data from the oscilloscope every second during the run period of each trial.

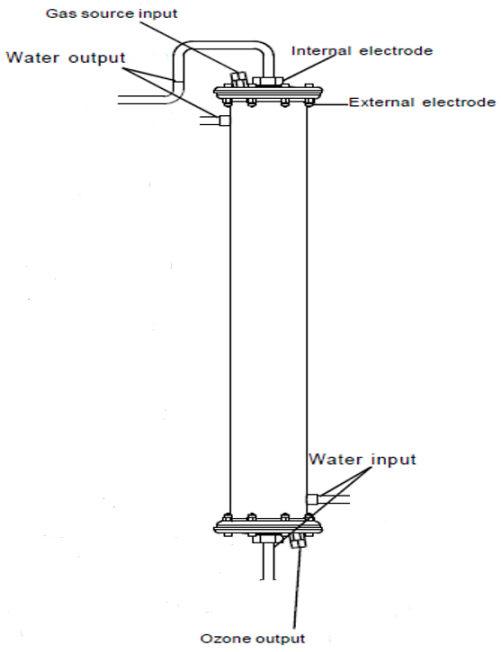

Figure 13. Reactor Schematic. Adapted from C. Diminick, Seton Hall alumni, Presentation material, not dated.

The reactor schematic, shown in Figure 13, features the gas (oxygen) input and ozone output. The water input and output for the inner electrode, and the outer electrode is shown as well. The reactor is composed of stainless steel tube (alloy $1.4404/316L$) which corresponds to the industry standard ozonizers as seen in Figure 14-(a) [50].
The inner tube of the reactor was a standard, ceramic coated, high voltage electrode placed into the exterior tubes which acted as ground electrode. The outer electrode was 24 inches long and 4 inches high; the gap separation between inner and outer electrode

(a) Reactor.

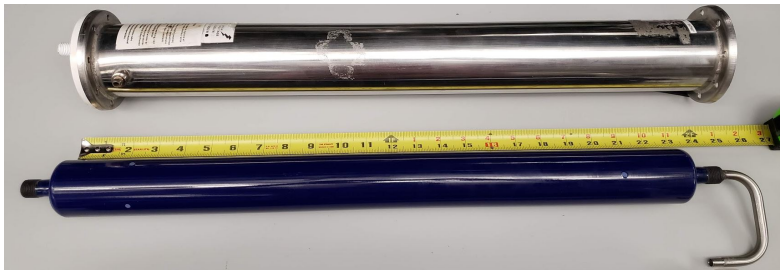

(b) Inner and outer electrodes.

Figure 14. a) Reactor. Gustavo, Duarte. 2020. JPG file. b) Inner electrode, ceramic coated. Gustavo, Duarte. 2020. JPG file.

was measured and was 3 mm as shown in Figure 14-(b).

A cooling water jacket was mounted inside the inner electrode to remove heat from the gap by convection. The process of cooling the inner electrode is novel, and the area of study as seen in Figure 15. The outer electrode was cooled as well, using the standard of the industry. Furthermore, in our system, we can cool both electrodes at the same time or each electrode by itself. In the experiment we use the data of the outer electrode as standard or ground level, since the industry uses this setup for cooling the gap.

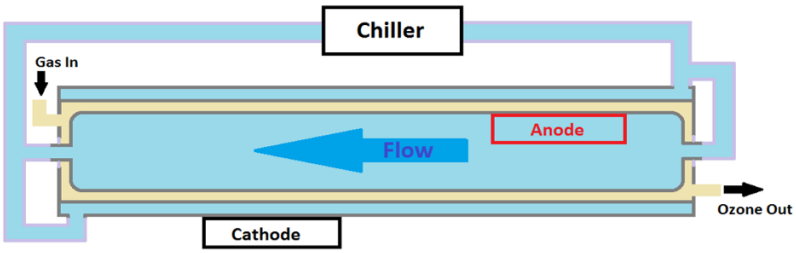

Figure 15. Reactor inner and outer electrodes. Schematic by M. Feurer, Seton Hall alumni, Presentation material, not dated.

The experiment was conducted under standard conditions of pressure and temperature. The rate flow of the gas was set at 1 liter per minute (L/min), 2 L/min, 3

L/min and 5 L/min. The chiller temperatures were set at $5°C$, $20°C$ and $35°C$ for the inner electrode, the outer electrode, and both electrodes as well. The duration of each run to collect data was set at 120 minutes or 180 minutes for each trial. After shutting off the power to the reactor, before running the next test, we allowed the reactor to re-equilibrate. We flowed pure O_2 through the system after shutting off power, in order to flush out residual ozone. The oscilloscope was set to measure total applied Voltage (Peak-to-Peak) across the entire circuit (V-AC), $V_{(RMS)}$ and $I_{(RMS)}$. We used 5.0 MS/sec (million samples per second) with Waveform Averaging of 32 or higher. Also, a signal trigger was set for the applied voltage and put it on DC. The scope was properly grounded. The applied voltage frequency of the current (PSU) was 2295 Hz. For the following measurements. The following data was collected every 10 minutes: apparent power (VA), wattage, power factor, line current draw ($Amps$).

5 Results and Analysis

The weight by weight percentage of ozone production vs time is shown in Figure 16. The gas flow rate is 1 liter per minute (L/min). Both electrodes are cooled at the same temperature during the running time of 2 hours. But, the temperature was adjusted to $7°C$, $10°C$, $13°C$, $16°C$, $19°C$ and $22°C$. When the temperature of the chiller is $7°C$ the ozone yield is in the order of 15 $\%$ $[wt/wt]$ and production is increasing during the trial without reaching a stable state or declining state. At $22°C$, the ozone production is in the order of 13.5 $\%$ $[wt/wt]$ and production is mainly linear at different periods of time. The other temperatures follow a similar trend. Taking into account the different temperatures, we observed that the production of ozone increases with the decreases of temperature.

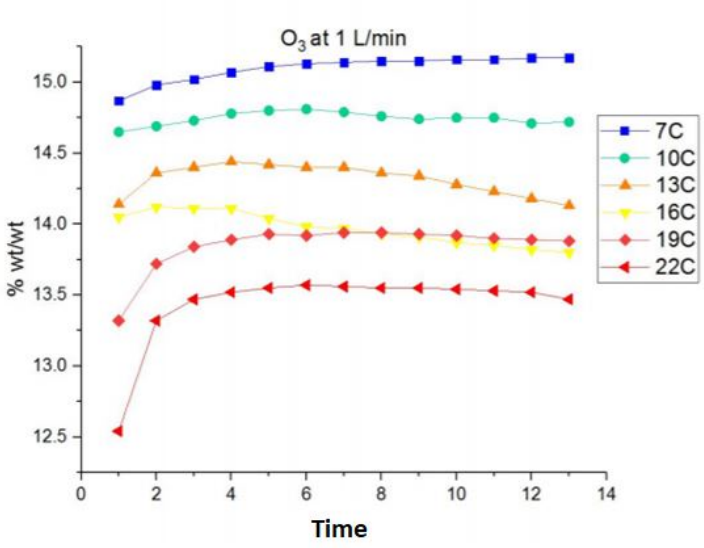

Figure 16. Ozone production, cooling both electrodes at a gas flow rate of 1 L/min. Data recorded every 10 minutes.

Figure 17 shows a gas flow rate of 2 L/min. Both electrodes are cooled at the same temperature during the running time. In this case, when the temperature is $5°C$ the ozone yield is in the order of 16 $\%$ $[wt/wt]$ and production is decreasing with a slower pace during the trial. At $35°C$, the ozone production starts in the order of 12 $\%$ $[wt/wt]$ but ends at 9 $\%$ $[wt/wt]$. A similar trend is observed at $20°C$ and $30°C$.

Figure 18 shows a gas flow rate of 3 L/min. Both electrodes are cooled at the same

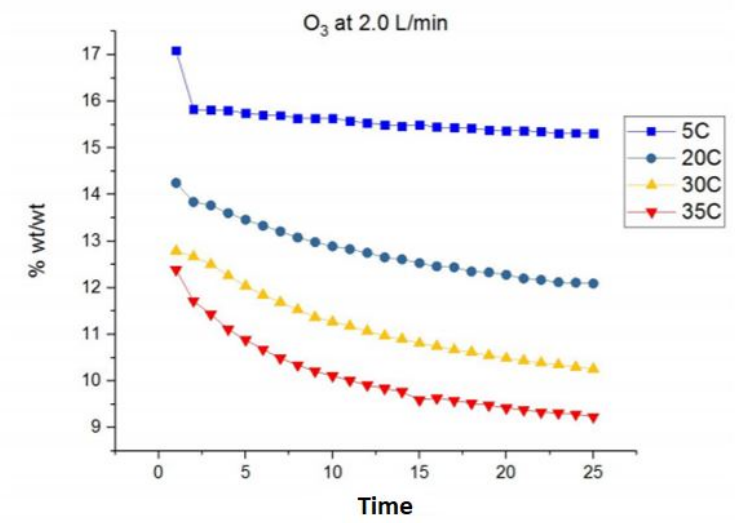

Figure 17. Ozone production, cooling both electrodes at a gas flow rate of 2 L/min. Data recorded every 5 minutes.

temperature during the running time of 2 hours. When the temperature of the chiller is at $7°C$, the ozone yield starts in the order of 10.3 $\%$ $[wt/wt]$ but ends at 10.1 $\%$ $[wt/wt]$. At higher temperatures the decline of ozone yield changes drastically with the increase of time. In the case of $19°C$, it goes from 9.9 $\%$ $[wt/wt]$ to less than 9.2 $\%$ $[wt/wt]$.

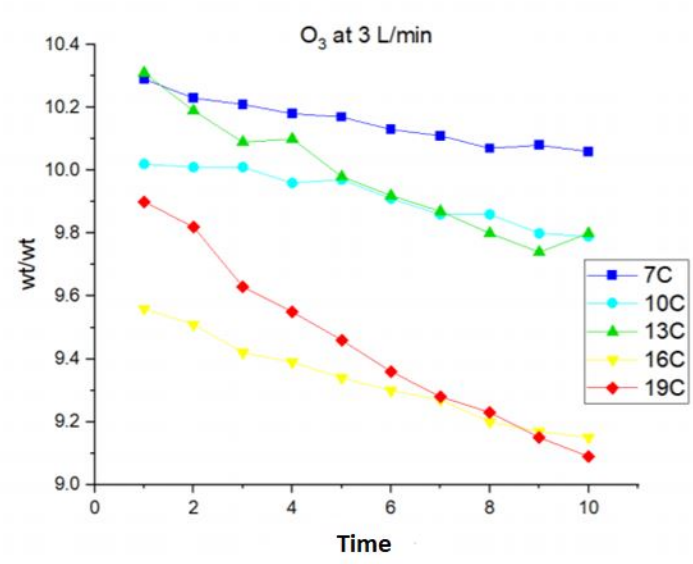

Figure 18. Ozone production, cooling both electrodes at a gas flow rate of 3 L/min. Data recorded every 12 minutes.

Figure 19 shows a gas flow rate of 5 L/min. Both electrodes are cooled at the same

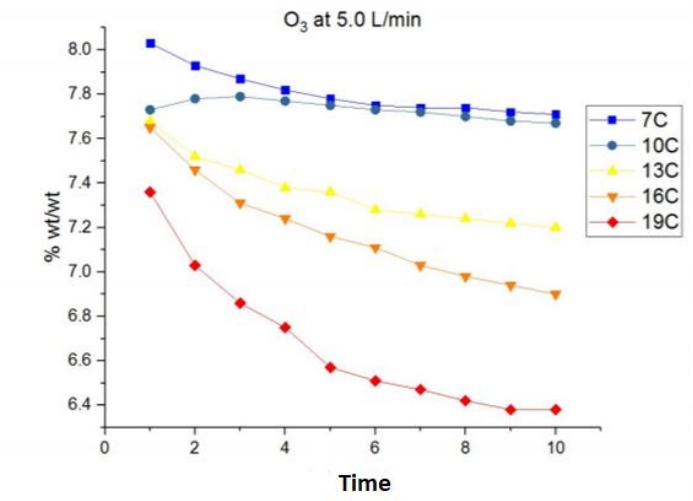

Figure 19. Ozone production, cooling both electrodes at a gas flow rate of 5 L/min. Data recorded every 12 minutes.

temperature during the running time of 2 hours. When the temperature is at $7°C$, the ozone yield starts in the order of 8 $\%$ $[wt/wt]$ but decreases slowly to 7.8 $\%$ $[wt/wt]$. At higher temperatures the decline of ozone yield changes drastically with the increase of time. At $19°C$, it goes from 7.4 $\%$ $[wt/wt]$ to less than 6.4 $\%$ $[wt/wt]$.

5.1 O_3 Production of Outer Electrode, Inner Electrode and Both Electrodes at the Same Time

The weight by weight percentage of ozone production vs time is shown in Figure 20. The gas flow rate is 1 liter per minute (L/min). The electrodes are cooled at the same temperature during the running time of 3 hours. But, the temperature was adjusted to $5°C$, $20°C$ and $35°C$. These conditions remain the same for ozone production in Figures 21 and 22. However, Figure 20 refers to the data obtained when cooling the outer electrode. When the temperature of the chiller is $5°C$, the ozone yield is on the order of 14.5 $\%$ $[wt/wt]$ and production is increasing during the trial without reaching a stable state or declining state. At $20°C$, the ozone production is in the order of 13.5 $\%$ $[wt/wt]$ and production is mainly linear, at different periods of time. At $35°C$, the ozone production is in the order of 11.5 $\%$ $[wt/wt]$ and production is increasing during

the trial. We observed that the production of ozone increases with the decreases of temperature.

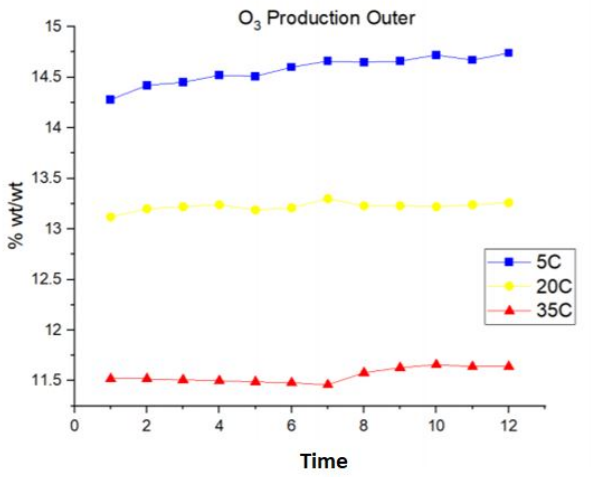

Figure 20. Ozone production, cooling the outer electrode with a gas flow rate of 1 L/min. Data recorded every 15 minutes.

Figure 21 shows weight by weight percentage of ozone production vs time when cooling the inner electrode. In this case, when the temperature is $5°C$; the ozone yield is on the order of 14.75 $\%$ $[wt/wt]$ and production is increasing without reaching a stable state or declining state. At $20°C$, the ozone production is in the order of 13.25 $\%$ $[wt/wt]$ and the production curve follows a similar trend as $5°C$. At the temperature of $35°C$, the ozone production is on the order of 11.75 $\%$ $[wt/wt]$ and production is increasing during the trial.

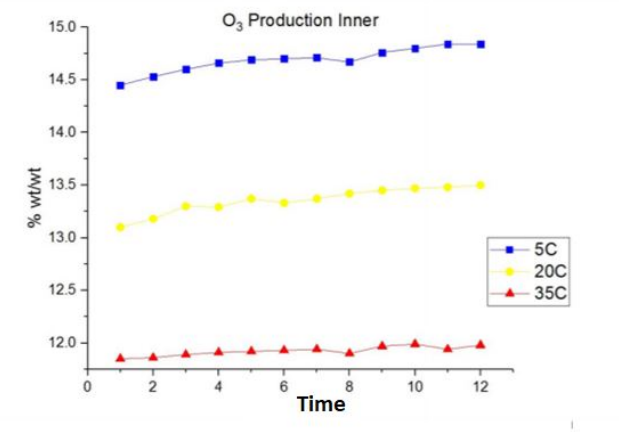

Figure 21. Ozone production, cooling the inner electrode with a gas flow rate of 1 L/min. Data recorded every 15 minutes.

Figure 22 shows weight by weight percentage of ozone production vs time. Both electrodes, inner and outer are cooled simultaneously at the same temperature during the running time. In this case, when the temperature is $5°C$, the ozone yield is on the order of 15.6 $\%$ $[wt/wt]$ and production is decreasing with time. At $20°C$, the ozone production is in the order of 14 $\%$ $[wt/wt]$ and production is increasing without reaching a stable state or declining state. At $35°C$, the ozone production is on the order of 12.25 $\%$ $[wt/wt]$ and production is increasing during the trial.

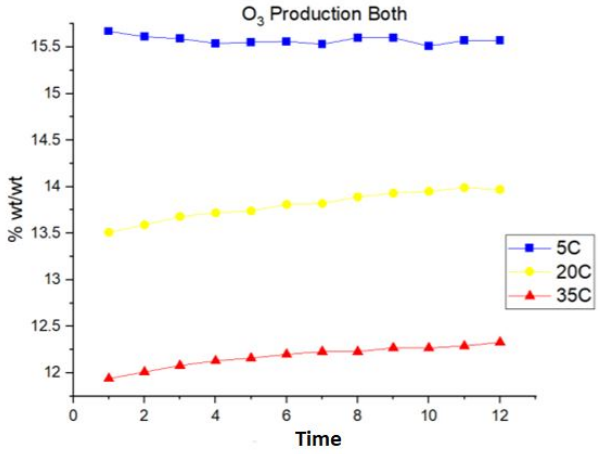

Figure 22. Ozone production, cooling both electrodes with a gas flow rate of 1 L/min. Data recorded every 15 minutes.

Table 7. O_3 yield side by side comparison.

O_3 Production	$5°C$	$20°C$	$35°C$
Outer	-	-	-
Inner	0.78 % $[wt/wt]$	2.87 % $[wt/wt]$	6.90 % $[wt/wt]$
Both	6.89% $[wt/wt]$	4.38 % $[wt/wt]$	9.28 % $[wt/wt]$

Table 7 shows a side by side comparison between the different temperatures vs cooling the outer electrode, inner electrode and both electrodes at the same time. Since cooling the outer electrode is the standard in the industry, we take the outer electrode as the ground level or 0 level. Notice, that cooling the inner electrode produces an increase in ozone yield $\%$ $[wt/wt]$. But, the larger increase occurs at $35°C$ in the order of 7 $\%$ $[wt/wt]$. When both electrodes are cooled at the same time the increase of ozone yield is on the order of 7 $\%$ $[wt/wt]$ at $5°C$ but almost 9.3 $\%$ $[wt/wt]$ at $35°C$.

5.2 $V_{(RMS)}$

The voltage root mean square value $V_{(RMS)}$ measured at the oscilloscope vs time is shown in Figure 23. The gas flow rate is 1 (L/min). Only the outer electrode is cooled, at the same temperature, during the running time of 3 hours. But the temperature was adjusted to $5°C$, $20°C$ and $35°C$. The conditions remain the same for Figures 24 and 25. When the temperature of the chiller is $5°C$, the V_0 average is 2322 V. At $20°C$, the V_0 average is 2231 V. Finally, at $35°C$, the V_0 average is 2140 V. Therefore, we observe an increment in the V_0 when the reactor is running at lower temperatures.

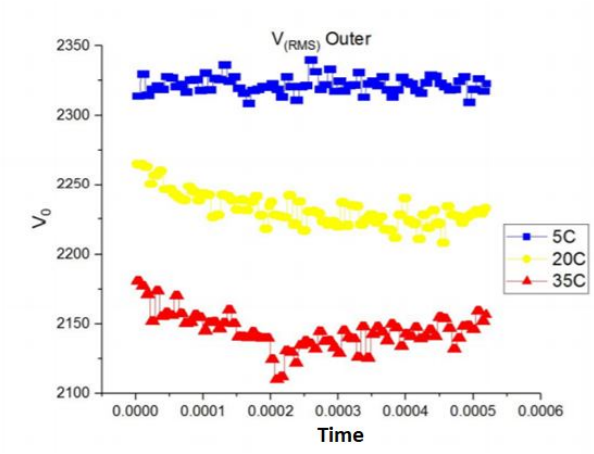

Figure 23. $V_{(RMS)}$ output for the outer electrode cooling. Screenshot of the oscilloscope taken every 10 minutes over a period of 3 hours.

The voltage root mean square value $V_{(RMS)}$ vs time is shown in Figure 24 when cooling the inner electrode. When the temperature of the chiller is $5°C$, the V_0 average is 2347 V. At $20°C$,the V_0 average is 2250 V. At $35°C$, the V_0 average is 2150 V. Therefore, we observe an increment in the V_0 used by the reactor at lower values of temperature. A similar trend was observed when cooling the outer electrode alone.

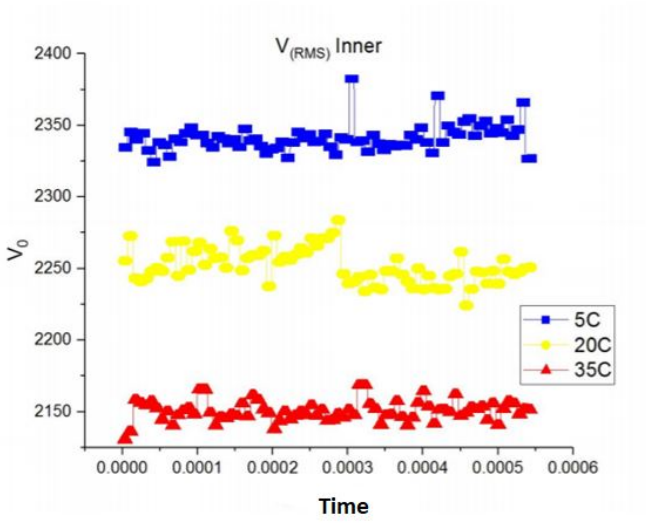

Figure 24. $V_{(RMS)}$ output for the inner electrode cooling. Screenshot of the oscilloscope taken every 10 minutes over a period of 3 hours.

The $V_{(RMS)}$ vs time is shown in Figure 25. Both electrodes, the inner and outer, were cooled at the same temperature during the running time. When the temperature of the chiller is $5°C$, the V_0 average is 2190 V. At $20°C$, the V_0 average is 2046 V. At $35°C$ the V_0 average is 1828 V. We observed an increment in the V_0 used by the reactor at lower temperatures.

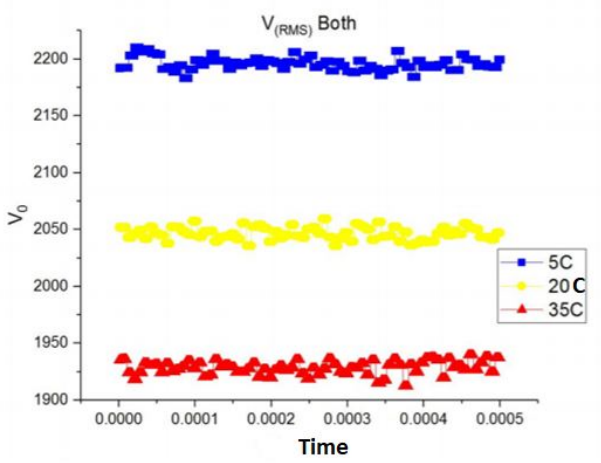

Figure 25. $V_{(RMS)}$ output for both electrodes cooling. Screenshot of the oscilloscope taken every 10 minutes over a period of 3 hours.

5.3 Other Measurements and Analysis

Table 8 shows the current measured at the oscilloscope vs temperature for each electrode and both electrodes at the same time. A trend is manifest where the lower temperature uses more current than the higher temperatures. Nevertheless, the difference is small and accounting for error and standard deviation shows no significant changes occur with the current.

Table 8. Current vs. Temperature.

	$5\ C$	$20\ C$	$35\ C$
Outer	$0.1616\ A$	$0.1605\ A$	$0.1592\ A$
Inner	$0.1613\ A$	$0.1598\ A$	$0.1580\ A$
Both	$0.1570\ A$	$0.1543\ A$	$0.1533\ A$

As expressed in the experiment setup section, other data set were collected such as peak to peak or apparent power ($V\,A$) to name a few. However, we did not report these results at this time because some parameters are related to V_0 or the changes were not significant enough to be reported. An interesting result is shown in Figure 26. We observed the inner tube with physical deposition of material. The powder deposited on the electrodes occurs during the reactor live operation which is calculated to be in the range of 300 to 400 hours. This powder could be fragments of metals sputtered out of the bulk material of the discharge tube by the high energy ions present in the discharge gap while the plasma is 'on'. However, notice that equivalent result was obtained by Bonitz et al. [3].

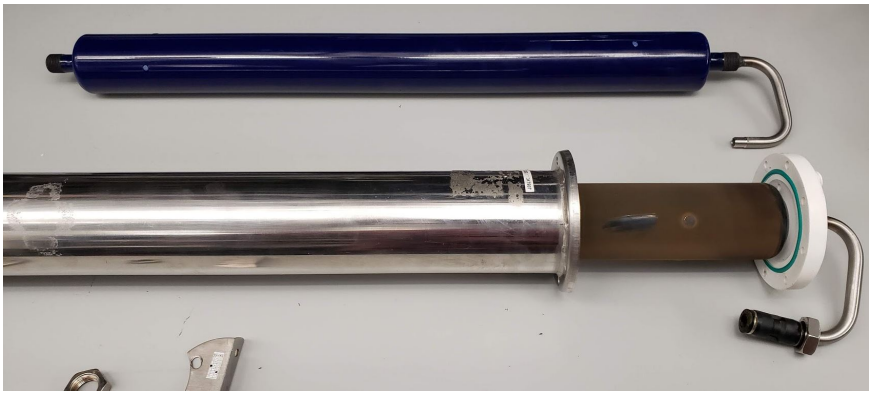

Figure 26. Deposition of material in the inner electrode. Gustavo, Duarte. 2020. JPG file.

Figure 27 shows a clear picture of the influence of gas flow rate on ozone production vs gas flow rate. We observe under $7°C$ a considerable decrease of ozone yield with the increase of gas flow from 1 liter per minute to a 5 liter per minute. A similar result was obtained by Zhang, et al. [45]. This decrease is due to the gas having less contact time with the discharge when the airflow is incremented. Notice that at 1 L/min ozone yield is in the order of 18 $\%$ $[wt/wt]$. At 3 L/min the ozone yield decreases near to 10 $\%$ $[wt/wt]$ which is a reduction of 4 $\%$ $[wt/wt]$ per liter added at the flow rate. At 5 L/min the ozone yield decreases near to 8 $\%$ $[wt/wt]$, a reduction of 2.5 $\%$ $[wt/wt]$ per liter added at the flow rate. The ozone reduction yield is more severe in the initial transition from 1 L/min to 3 L/min than in the second one from 3 L/min to 5 L/min. Nevertheless, we observed a linear relationship between ozone production and flow rate.

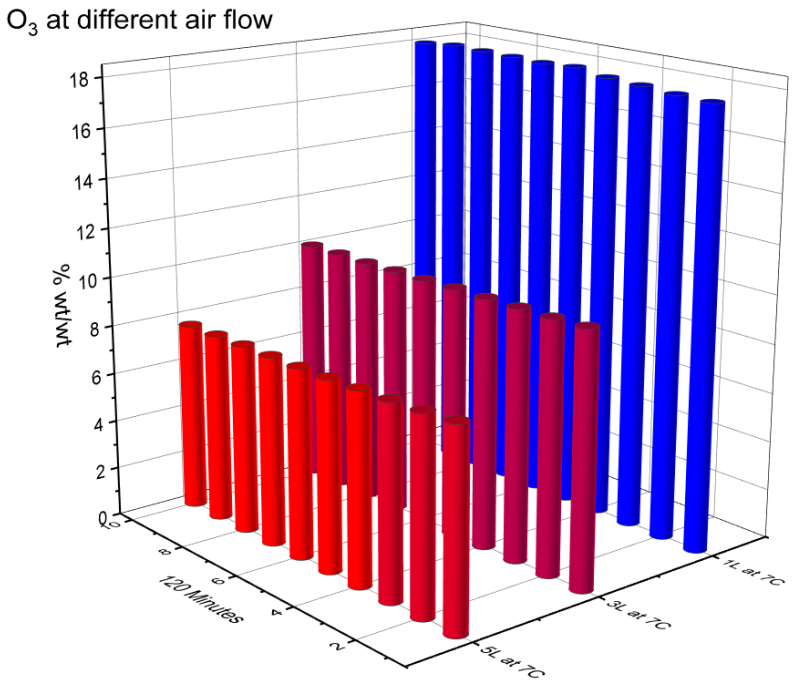

Figure 27. Ozone production cooling both electrodes at different gas flow rates, at same temperature.

Figure 28 shows the ozone output for the cooling of the outer electrode, inner electrode and cooling both electrodes at the same time vs temperature. Moreover the figure shows the difference of ozone output at different temperatures for each configuration. We observed in each case that the ozone yield is higher for $5°C$ than $20°C$. A similar result was obtained by Nassour, et al. [46]. The ozone yield increases at lower

temperatures because heat is removed from the discharge gap by water convection and conduction. Furthermore, we observed that inner and outer electrodes cooling processes have similar output characteristics. When cooling both electrodes the output of ozone increases by almost 7 $\%$ $[wt/wt]$ at $5°C$ and 5 $\%$ $[wt/wt]$ at $20°C$.

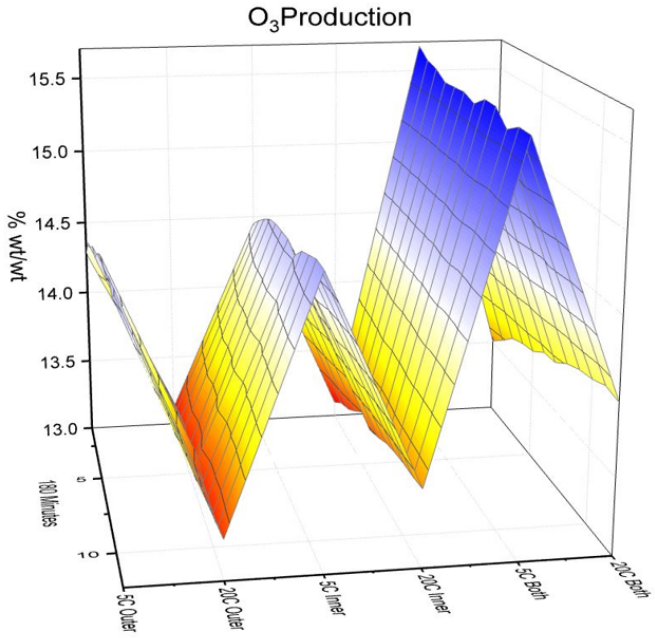

Figure 28. O_3 Production for different electrodes cooling configuration.

The increase of ozone production at lower temperature is due to various variables. The decrease in temperature also decreases the velocity of the species in the reactor. Velocity and energy are related to changing the reaction path of ozone reactions. Decreasing the number of excited species in the plasma leads to an increment of ozone because excited species tend to destroy the ozone molecules [47]. When the temperature increases the opposite is observed. Furthermore, the ozone yield is related to variables such as the secondary Townsend Coefficient, the reduced electric field, the relative atom concentration and thermal pressure relationship to name a few. Most of these variables have a direct or indirect relationship with temperature. Nonetheless, a linear relationship between ozone production and temperature was observed.

Figure 29 shows the V_{RMS} reading from the oscilloscope vs temperature. The figure also shows the V_{RMS} reading for each electrode configuration at different temperatures. We observed in each case that V_{RMS} is higher for $5°C$ than $20°C$ and $35°C$. We observed that inner and outer cooling processes have similar V_{RMS} characteristics. When both electrodes are cooled the V_{RMS} is lower than the other configurations.

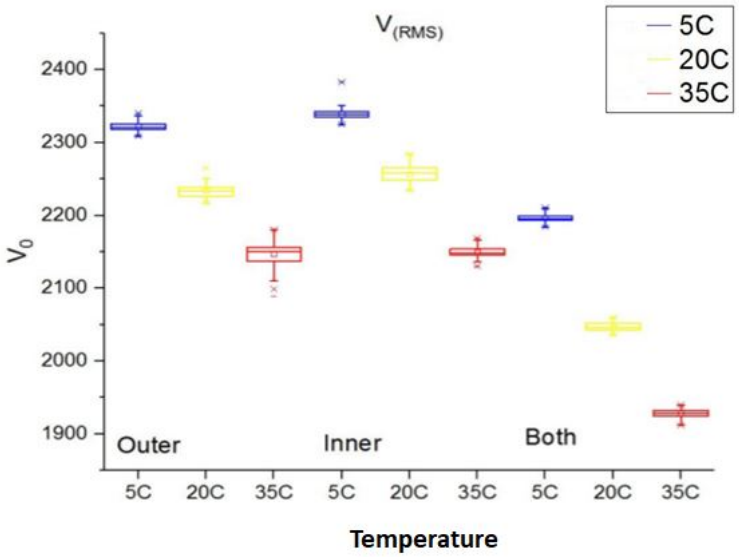

Figure 29. V_{RMS} for different electrodes cooling configuration.

The increase of V_{RMS} at lower temperature is due to various parameters. These parameters are the energy of the excited state of the species, the vibrational and rotational energy. We must also contemplate the reaction path of the species, the secondary Townsend Coefficient, configuration of the electrodes and materials to name a few. Furthermore, the walls of the electrodes are partially responsible for the V_{RMS} increase at lower temperatures [48]. The deposition of materials in the inner electrode affects directly the reduced electric field. Nonetheless, we observed a linear relationship between, V_{RMS} and temperature for the different electrode configuration.

6 Concluding Remarks

This Thesis has provided an introduction to the theory of Plasma Physics and Dielectric Barrier Discharge. We have discussed the mechanism of plasma formation such as direct ionization or ion-ion recombination to name a few. Also, we discussed the Townsend process, the formation of streamers and micro-discharges. We learned the basis of Dielectric Barrier Discharge such as the different configurations, Lissajous figure and electrical properties. We learned the theory behind ozone formation and chemical reactions. We reviewed the literature from the main authors on the field. We specifically reviewed literature related to effects of cooling in ozone production and reactors characteristics.

We present a novel DBD reactor with the capability of cooling the inner electrode only, the outer electrode only and both electrodes at the same time. We found out that cooling both electrodes improves the ozone production by almost 7 $\%$ in comparison with the industry standard. We noted a linear relationship between ozone production and the gas flow rate; as the latter increases, the ozone yield decreases. A linear relationship between ozone production and temperature is outlined by the data collected. The data shows an increase in the ozone yield as the temperature decreases. We also found out that the voltage increases as the temperature decreases. The increase of voltage is related to various factors such as energy of the species or reduced electric field. We also discovered that a deposition of material in the inner electrode may suggest changes of the electric field. Furthermore, the accumulation of charges at the electrodes could play a significant role in the increase of voltage at lower temperature. Nevertheless, we found a linear relationship between voltage and temperature.

The cooling of the inner electrode and the outer electrode combined produced more ozone than the market standard. But notice that having water on the inner electrode (high voltage) is a source of possible corrosion of the dielectric. The risk of water leaks on the inner (high voltage) electrode could be catastrophic for the reactor. Nevertheless, more research is needed to understand the consumption of energy at the reactor; the effects of voltage accumulation at lower temperatures and the relationship between

deposition and charge accumulation. Finally, Spectrometry could be used to better understand the influence of chemical reactions and the different species formed as the temperature changes in the system.

References

[1] Langmuir, I. Phys. Rev., 33: 954 (1929).

[2] Francis F. Chen. “Introduction to Plasma Physics and Controlled Fusion.” Third edition. Switzerland. Springer. Print, (2016).

[3] Michael Bonitz, Jose Lopez, Kurt Becker, Hauke Thomsen.“Complex Plasma.” Switzerland. Springer. Print, (2014).

[4] K. Hiragaki, et al. “Generation of Ozone Foam and Its Application for Sterilization.” Akaiwa-City, Japan. Published by INP Greifswald and IFP Greifswald (2014).

[5] F. Mitsugi, et al. “Application of Surface Barrier Discharge for Pest Control.” Kurokami, Kumamoto, Japan. Published by INP Greifswald and IFP Greifswald (2014).

[6] V.Yu Khomich, I.E. Rebrov, V.A. Yamshchikov. “Electrohydrodynamic Flow Induced by Dielectric Discharge for Gas Laser Circulation System.” Saint Petersburg, Russia. Published by INP Greifswald and IFP Greifswald (2014).

[7] M. Oneby, et al. “Ozone Treatment of Secondary Effluent at U.S. Municipal Wastewater Treatment Plants.” Milwaukee, USA. International Ozone Association (2010).

[8] H. Glaze, et al. “The Chemistry of Water Treatment Processes Involving Ozone, Hydrogen Peroxide and ultraviolet radiation.” Los Angeles, USA. International Ozone Association (1987).

[9] B. Loeb. “Ozone: Science & Engineering Thirty Years of Progress.” Cincinnati, USA. International Ozone Association (2009).

[10] Alfred Grill. “Cold Plasma Material Fabrication.” New York, New York. Published by Institute of Electrical and Electronic Engineers. Print, (1994).

[11] J.A. Bittencourt. “Fundamentals of Plasma Physics.” Third Edition. New York. Springer. Print, (2004).

[12] Venugopalan, M., ed. Reactions Under Plasma Conditions, Vol. I. New York. Wiley-Interscience, (1971).

[13] Alexander Fridman, Lawrence A. Kennedy. “Plasma Physics and Engineering.” Second Edition. Boca Raton, Florida. CRC Press Taylor & Francis Group. Print, (2011). pp. 15-26.,(*) pp. 206-214.

[14] Stephen M. Rossnagel, Jerome J. Cuomo, and William D. Westwood “In Handbook of Plasma Processing Technology.” Park Ridge, NJ. Noyes Publications (1990). p. 14.

[15] K.H. Becker, U. Kogelschatz, K.H. Schoenbach, R.J. Barker. “Non-Equilibrium Air Plasmas at Atmospheric Pressure.” London, United Kingdom. Published by Institute of Physics Publishing, wholly owned by The Institute of Physics, London. Print, (2005).

[16] Zecca A., Karwasz G. P. and Brusa R. S. Rivista del Nuovo Cirnento 19 I., (1996).

[17] Radzig A. A., and Smirnov B. B. Reference Data on Atoms, Molecules and Ions. Berlin. Springer (1985).

[18] M. Figus, Rotational and vibrational temperature measurements in capillary plasma electrode (CPE) discharges. Master’s Thesis, Steven Institute of Technology, QC718.5.S6 F54 (2004).

[19] Kossyi I. A., Kostinki A. Yu, Matveyev A., Silakov V. P. Plasma Sources Sci. Technol, 1207 (1992).

[20] Herron J. T. and Green D. S. Plasma Chem. Plasma Process., 21 459. (*) Tables [2-3-4]. (2001).

[21] Stefanovic I., Bibinov N. K., Deryugin A. A., Vinogradov I. P., Narpatovich A. P. and Wiesemann K. Plasma Sources Sci. Technol, 10 406 (2001).

[22] W. Siemens, Poggendorff 's Ann. Phys. Chem. 102, 66 (1857).

[23] T.C. Manley " The electric characteristics of the ozonator discharge." Electrochem. Soc. 84(1)., (1943). (*) pp 83-96.

[24] Klemenc A., Hinterberger H., and Hofer H. Z. Elektrochem., 43 708-712 (1937).

[25] Suzuki M. and Naito Y. Proc. Jpn. A cad., 2469-476 (1952).

[26] Gobrecht H., Meinhardt O. and Hein F. Bunsenges. Phys. Chern. Berlin, 68 55-63 (1964).

[27] Bagirov M. A., Nuraliev N. E. and Kurbanov M. A. Sov. Phys.-Tech. Phys., 17495-498 (1972).

[28] B. Eliasson, Senior Member, IEEE, and Ulrich Kogelschatz. "Nonequilibrium Volume Plasma Chemical Processing." IEEE Trasactions on Plasma Science, Vol. 19, No. 6, December (1991).

[29] S. Stucki (ed) Process Technologies for Water Treatment. New York. Plenum Press, pp 87-120. Plasma Chem. Plasma Process., 231-46 (1998).

[30] Falkenstein Z. and Coogan J. J. Journal Phys. D: Appl. Phys., 30 817-825 (1997).

[31] Blair D. T. A. and Whittington H. W. Journal Phys. D: Appl. Physics, 8 405-15 (1975).

[32] Shibuya Y. Proc. 3rd Int. Conf. Gas Discharges. IEEE Conf. Publ. No 181, pp 132-5. London (1974).

[33] Eliasson B. Kogelschatz U. and Hirth M. Proc. XVII Int. Conf. Phenomena in Ionized Gases, Budapest, ed. J S Bakos pp 590-2 (1985).

[34] B. Eliasson, M. Hirth and U. Kogelschat. "Ozone synthesis from oxygen in dielectric barrier discharge." J. Phys. D: Appl. Phys., 20 1421-1437. Printed in the UK (1987).

[35] Eliasson B, Kogelschatz U, Strassler S and Hirth M. Brown Boveri Research Report, No KLR 83-28 C (1983).

[36] M. Beitr. Plasma Phys., 20 1-27 (1981).

[37] Pollo I., Ozonek J. and Fijalkowski S. Proc. 7th. Int. Symp. Plasma Chemistry. Eindhoven, ed. C. J. Timmermans pp 407-11 (1985).

[38] S. Yagi and M. Tanaka. "Mechanism of ozone generation in air-fed ozonisers." J. Phys. D: Appl. Phys., Vol. 12. Printed in Great Britain (1979).

[39] Eliasson B. and Kogelschatz U. Proc. 8th Int. Symp. on Plasma Chemistry, ISPC-8. Tokyo, vol 2, pp 736-741 (1987).

[40] Kogelschatz U. and Baessler P. Ozone Sc. Eng., 9 195-206 (1987).

[41] Andrews T. and Tait P. G. Phi. Trans. Roy. Soc. London, 150 113 (1860).

[42] H. Sadat, N. Dubus, J. M. Tatibouët. "Temperature Runaway in a Pulsed Dielectric Barrier Discharge Reactor." Institut Prime, France (2011).

[43] Surapon Boonduang, Pichet Limsuwan. "Effect of Generating Heat on Ozone Generation in Dielectric Cylinder-Cylinder DBD Ozone Generator." Bangkok, Thailand. Energy and Power Engineering, 2013, 5, 523-527. Published Online November 2013. (http://www.scirp.org/journal/epe).

[44] Nicole Brueggemanna, et al. "Cooling Conditions of Ozone Generators." Herford, Germany. Ozone: Science & Engineering 2017, VOL. 39, NO. 3, 196–201. Taylor & Francis Group (2017).

[45] Yafang Zhang, Linsheng Wei, Xin Liang, and M. Šimek. "Ozone Production in Coaxial DBD Using an Amplitude-Modulated AC Power supply in Air." Ozone: Science & Engineering. Taylor & Francis Group (2018).

[46] Kamel Nassour, et al. “Comparative Experimental Analysis of Ozone Generation between Surface and Volume DBD Generators.” IEEE Transactions on Dielectrics and Electrical Insulation. Vol. 25, No. 2 (2018).

[47] Linsheng Wei, Min Xu, and Yafang Zhang. “Energy Conversion and Temperature Dependence in Ozone Generator Using Pulsed Discharge in Oxygen.” Nanchang, China. Ozone: Science & Engineering 2017, Vol. 39, No. 1, 33-3. Taylor & Francis Group (2016).

[48] Woo Seok Kang, Hyun-Su Kim, and Sang Hee Hong. “Gas Temperature Effect on Discharge-Mode Characteristics of Atmospheric-Pressure Dielectric Barrier Discharge in a Helium–Oxygen Mixture.” IEEE Transactions on Plasma Science, Vol. 38, No. 8 (2010).

[49] R. Peyrous, P. Pignolet, and B. Held, “Kinetic simulation of gaseous species created by an electrical discharge in dry or humid oxygen,” J.Phys. D, Appl. Phys., vol. 22, no. 11, pp. 1658–1667, Nov (1989).

[50] Sieghard Seyrling, Marco Muller, and Luca Ramoino. “Influence of reactor surface materials on the ozone zero phenomenon.” Published online 6 June 2017 – c EDP. Sciences, Societ‘a Italiana di Fisica, Springer-Verlag (2017).